REPORT DOCUMENTATION PAGE

Form Approved
OMB No. 0704-0188

1. REPORT DATE *(DD-MM-YYYY)*	2. REPORT TYPE	3. DATES COVERED *(From - To)*
06/07/2015	Final	01/09/2010-06/07/2015

4. TITLE AND SUBTITLE
Deterministic and advanced statistical modeling of wind-driven sea

5a. CONTRACT NUMBER

5b. GRANT NUMBER
N00014-10-1-0991

5c. PROGRAM ELEMENT NUMBER
N/A

6. AUTHOR(S)
Zakharov Vladimir
Pushkarev Andrei

5d. PROJECT NUMBER
14PR02254-00

5e. TASK NUMBER
N/A

5f. WORK UNIT NUMBER
N/A

7. PERFORMING ORGANIZATION NAME(S) AND ADDRESS(ES)
Waves and Solitons LLC,
1719 W. Marlette Ave.,
Phoenix AZ 85015-2037

8. PERFORMING ORGANIZATION REPORT NUMBER
N/A

9. SPONSORING/MONITORING AGENCY NAME(S) AND ADDRESS(ES)
Carol A. Porter, tel (703) 696-2587, EMAIL: Carol.porter@onr.mil
Office of Naval Research
875 North Randolf Street
Arlington VA, 22203-1995

10. SPONSOR/MONITOR'S ACRONYM(S)
ONR BD025

11. SPONSOR/MONITOR'S REPORT NUMBER(S)
N/A

12. DISTRIBUTION/AVAILABILITY STATEMENT
Approved for public release, distribution is unlimited

13. SUPPLEMENTARY NOTES
N/A

14. ABSTRACT
We propose new framework for numerical modeling of Hasselmann equation, based on exact nonlinear interaction term, new ZRP wind input term, absence of spectral maximum and presence of short-wave dissipation. We analyze five differen wind input term in the frame of new framework, and observe that only ZRP wind input term provides good correspondence with field experimental measurements and theory. Based on the idea of nonlinearity domination and self-similarity, we developed the set of tests allowing to subject to critical analysis any existing statistical surface waves model. We also developed and tested dynamical numerical model proving absence of spectral maximum dissipation.

15. SUBJECT TERMS
N/A

16. SECURITY CLASSIFICATION OF:			17. LIMITATION OF ABSTRACT	18. NUMBER OF PAGES	19a. NAME OF RESPONSIBLE PERSON
a. REPORT	b. ABSTRACT	c. THIS PAGE			Pushkarev Andrei
					19b. TELEPHONE NUMBER *(Include area code)*
U	U	U	UU	1	(602) 748-4286

20150720015

Waves and Solitons LLC

Letter of Transmittal

Waves and Solitons LLC, 1719 W. Marlette Ave., Phoenix, AZ 85015-2037

Phone: (602) 748-4286
Email: dr.push@gmail.com

Pushkarev Andrei
Member

Defense Technical Information Center
8725 John J Kingman Road Ste 0944
Fort Belvoir, VA 22060-6218

Dear Madam, Sir

I am pleased to provide you with the Final Technical Report for grant N00014-10-1-0991. The report covers the period from 1 September 2010 to 6 July 2015.

I certify that the attached Final Technical report is an honest and accurate account of the performed research.

Should you have any questions, please contact Pushkarev Andrei at (602) 748-4286, or E-mail: dr.push@gmail.com

Enclosure: Final Technical Report, standard form SF298

Sincerely,

Pushkarev Andrei, Member

July 6, 2015
Date

Final Technical Report

Deterministic and advanced statistical modeling of wind-driven sea

Vladimir Zakharov, Andrei Pushkarev

Waves and Solitons LLC, 1719 W. Marlette Ave., Phoenix, AZ 85015
phone: +1 (602) 748-4286 e-mail: dr.push@gmail.com

Award Number: N00014-10-1-0991

LONG TERM GOALS:

Development of accurate and fast advanced statistical and dynamical nonlinear models of ocean surface waves, based on first physical principles, which will improve and accelerate both long term ocean surface wave turbulence forecasts and prediction of strongly coherent events, such as freak waves and wave-breakings.

OBJECTIVES:

Creation of better statistical models for improvement of existing operational wave prediction programs; study of non-stationary waves growth in presence of wind; interpretation of experimental data through study of self-similar solutions of Hasselmann equation; studying the integrability of 1D dynamical equations for surface waves; study of the possibility of generalization of compact 1D water waves equation for 2D situation; study of the implications of modulational instability on solitons, rogue waves and air-surface interaction.

APPROACH

Numerical methods for solution of integro-differential equations; analytical self-similar solutions for integro-differential equations; Hamiltonian formalism; comparison of analytical and numerical solutions with experimental data; analytical and numerical solution of approximate models for deep water surface waves

WORK COMPLETED:

- We propose to use new wind forcing source term, which is analytical solution of Hasselmann equation, consistent with experimental data and numerical simulation
- We prove that there is no reason to include dissipation in the spectral maximum area. Instead, we justify localization of dissipation in high wave-numbers area
- We re-examine energy balance in the wind-driven sea and find that the major term in the energy balance is nonlinear interaction term S_{nl}. This fact explains Kolmogorov-Zakharov

weak-turbulent spectra $I_\omega \sim \omega^{-4}$ and $I_\omega \sim \omega^{-11/3}$ and self-similar behavior both in experimental observations and numerical simulation as well

- We propose new framework for simulation of Hasselmann equation based on exact nonlinear interaction term in Webb-Resio-Tracy (*WRT)* form, new wind input term and wave-breaking damping localized in high wave-numbers
- We found that majority of field and wave tank experimental data can be explained in terms of self-similar solution of the Hasselmann kinetic equation. The self-similarity explains persistence of the "magic links" connecting indices of energy and mean frequency dependencies in fetch- and duration-limited setups
- We analyzed proposed alternative framework for HE simulation through massive numerical experiments of Hasselmann equation and found that they reproduce more than a dozen of field experiments
- Based on the idea of nonlinearity domination and self-similarity, we developed the set of tests allowing separating physically based wind input terms from non-physical ones
- We show that central role of self-similar regimes explains very simple "universality of the wind-driven sea", connecting average steepness, frequency of the spectral peak and fetch. This universality is observed in majority of field and wave tank experiments. This is strong confirmation of our basic concepts
- We propose and compare with the original exact 1D Euler dynamical equation their cost-effective simplifications
- We analyze relation of modulational instability and coherent events such as solitons and freak waves
- We study the peculiarities of breaking waves and air flow interaction, allowing to understand air structures formation and their influence on surface waves

1. Nonlinearity domination in Hasselmann equation and alternative framework of its numerical simulation

The motivation of the research presented in current report was to continue the project of finding firm scientific foundation for study of wind driven seas.

The most important step in this direction was made in 1962 by K. Hasselmann [R2,R3] who proposed kinetic equation for wind waves description

$$\frac{\partial \varepsilon}{\partial t} + \frac{\partial \omega_k}{\partial \vec{k}} \frac{\partial \varepsilon}{\partial \vec{r}} = S_{nl} + S_{in} + S_{diss} \tag{1}$$

similar to equations used in condensed media physics starting since 1920-ies, where $\varepsilon = \varepsilon(\omega_k, \theta, \vec{r}, t)$ is the wave energy spectrum as a function of wave dispersion $\omega_k = \omega(k)$, angle θ, two-dimensional real space coordinate **Error!**=(x, y) and time t. S_{nl}, S_{in} and S_{diss} are nonlinear, wind input and wave-breaking dissipation terms correspondingly. Hereafter only the deep water $\omega_k = \sqrt{gk}$ case is considered, where g is the gravity acceleration and k=|**Error!**| is the absolute value of the wave number $\vec{k} = (k_x, k_y)$.

Eq. (1) is widely accepted in the oceanographic community [R4,R5] and has several names. It is called the Boltzmann equation [R5] (while this is not exactly correct), the energy balance equation [R4] and the radiation balance equation. We will call it the Hasselmann equation (hereafter *HE*) as a tribute to Hasselmann's pioneering work. At least the part of the community uses the same terminology [R6].

The right side of the Eq. (1) consists of three terms. The S_{nl} term is completely known. It was consistently derived from Euler equations and describes resonant interaction of quadruplets of waves satisfying

$$\vec{k} + \vec{k}_1 = \vec{k}_2 + \vec{k}_3 \tag{2}$$

$$\omega_k + \omega_{k_1} = \omega_{k_2} + \omega_{k_3} \tag{3}$$

Traditionally for theoretical physics, S_{nl} is represented in the form

$$S_{nl}(\omega,\theta) = F(\omega,\theta) - \Gamma(\omega,\theta)\varepsilon(\omega,\theta) \tag{4}$$

Here F is essentially positive "income term", presenting density of the energy flux into specific wave "at the expense" of other waves. The negative term $-\Gamma(\omega,\theta)\varepsilon(\omega,\theta)$ is the "offtake term" responsible for energy transfer to other waves due to nonlinear interactions. The explicit expressions for F and Γ are not presented due to their complexity. One can find them in multiple publications, for example [R7,R8]. In thermodynamics, the equilibrium between "income term" and "offtake term" provides formation of thermodynamically equilibrium spectra - Maxwell and Plank distributions.

The function Γ also has another physical sense. In presence of nonlinear wave ensemble, the dispersion law is undergoing the renormalization

$$\omega_k \to \omega_k + \Delta\omega_k \tag{5}$$

The renormalization has real and imaginary parts. The imaginary part is

$$\mathrm{Im}\,\Delta(\omega) = \frac{1}{2}\Gamma(\omega,\theta) \tag{6}$$

Thus, the S_{nl} term is reliably known. Opposite to it, the "source function" S_{in} – energy income from the wind and its dissipation function S_{diss} due to wave-breaking are known just approximately. There is no consensus regarding their form in oceanographic community. We discuss these questions in Sections 2 and 3 of current report. Meanwhile, the numerical experiments show that wind waves level is sensitive to the individual choice of the source function. The ambiguity of their proper definitions presents first major difficulty for wind wave theory and effective operational models development as well.

The second difficulty is connected with S_{nl} collision term numerical simulation. It is complex non-linear operator having, meanwhile, deep internal symmetry. Several S_{nl} simulation algorithms are

available at the moment: Webb-Resio-Tracy (*WRT*) [R9,R10], Lavrenov [R11], Masuda [R12]. All of them provide reliable results, but are too slow to provide simultaneous *HE* solution of the Eq. (1) in the dozen thousands points faster than real time, as it is required by operational wave forecasting. Because of that, existing operational models use much faster substitutes of S_{nl} in the form of *DIA* and its analogs, which leads to appearance of new undefined parameters which needs to be "tuned". In a sense, using of such tuning parameters presents, in particular, an attempt to "undo" the damage incurred to the model through substitution of S_{nl} by *DIA*.

As a result, all existing operational models need to be "tuned-up" for any individual set-up. Even if this situation is satisfactory from the engineering viewpoint, any further attempts of these models improvement do not provide any real progress in understanding of the processes of the ocean surface physics, and seem rather futile. It is necessary therefore to radically change the methodology and place it on solid scientific background.

First of all, correct definition of the source functions is necessary. It's possible to do that without new theoretical constructions and new difficult experiments. It is sufficient just to use existing experimental data in proper way. For 68 years, starting from well-known work of Sverdrup and Munk [R13], physical oceanography has accumulated plethora of experimental facts regarding wave growth speed at certain wind. Part of those facts was obtained in water tanks, but the most interesting are the ocean measurements.

Nowadays, the results of more than two dozens of measurements related to the "fetch limited" field set-ups, when off the shore wind and waves are quasi-stationary, are systemized and published. All those situations are described by stationary *HE*

$$\frac{\partial \omega_k}{\partial k}\frac{\partial \varepsilon}{\partial x} = S_{nl} + S_{in} + S_{diss} \tag{7}$$

This equation was solved in the presented research for different source functions S_{in} and S_{diss}. Five experiments were carried out for different wind input functions, and their results were compared to known ocean field experimental data. This comparison actively used the fact that the results of those experiments are well described by weak turbulence theory (*WTT*). This theory is well explained in details in monograph [R14], and applications of this theory to the ocean experiments are presented in publications [R15, R8,R16, R17, R18, 19] [R8,R15-R19].

The possibility of *WTT* application is based on the fact that S_{nl} in Eq. (1) is the dominant term. This fact can be explained in the following way. All S_{in} cases considered in current research are quasi-linear ones, which means that

$$S_{in} = \gamma(\omega,\theta)\varepsilon(\omega,\theta) \tag{8}$$

$$S_{diss} = -\gamma_{diss}(\omega,\theta)\varepsilon(\omega,\theta) \tag{9}$$

Taking into account S_{nl} splitting Eq. (4), Eq. (7) take the form

$$\frac{\partial \omega_k}{\partial \vec{k}}\frac{\partial \varepsilon}{\partial \vec{r}} = F(\omega,\theta) - (\Gamma(\omega,\theta) - \gamma(\omega,\theta) + \gamma_{diss}(\omega,\theta))\varepsilon(\omega,\theta) \tag{10}$$

One should note that γ typically has fairly small value $10^{-5}\omega_p$ for waves with the frequencies close to the peak frequency ω_p. The value of γ_{diss} does not exceeds γ, or waves are not excited at all. Meanwhile, the value of Γ is rather big, as show analytic and numeric calculations. It easily overlaps γ by more than the order of magnitude [R7,R20]. Therefore, one can substitute in the first approximation Eq. (10) by conservative equation

$$\frac{\partial\omega_k}{\partial k}\frac{\partial\varepsilon}{\partial x} = S_{nl} \tag{11}$$

which is, indeed, the subject of the *WTT* study.

It is customary to use "Kitaigorodsky dimensionalization", where the fetch variable x, total energy E and peak frequency ω_p are substituted by dimensionless variables

$$\chi = \frac{xg}{u^2}, \quad \varepsilon = \frac{Eg^2}{u^2}, \quad \hat{\omega} = \frac{\omega_p u}{g} \tag{12}$$

All ocean and wave tank measurements show that $\varepsilon(\chi)$ and $\omega(\chi)$ are power functions of dimensionless fetch

$$\varepsilon = \varepsilon\chi^p \tag{13}$$

$$\hat{\omega} = \omega_0\chi^{-q} \tag{14}$$

The values of p and q are varying in different experiments, but not in significant limits: $0.74<p<1$, $0.2<1<0.3$. They are connected with the good accuracy by "magic relation"

$$10q - 2p = 1 \tag{15}$$

These facts are explained by *WTT* [R15]. Conservative kinetic Eq. (11) has 4-parameter family of self-similar solutions [R16,R17], for which the "magic relation" is fulfilled exactly.

It was shown in [R1] that non-conservative *HE* with dissipation localized in short waves and forcing chosen in the power function form

$$\gamma(\omega,\theta) = f(\theta)\omega^s \tag{16}$$

also allows self-similar solution. It preserves the "magic relation" Eq. (15) as well.

All the numerical experiments presented in current report included short-wave dissipation, but in the "implicit" way: the spectrum at frequencies $f>1.1Hz$ has been changed to Phyllips spectrum $\varepsilon \sim \omega^{-5}$. The validity of this approach is discussed in the Section 3.

Four out of five of those experiments assumed absence of long-wave dissipation in longer waves. Such experimental set-up contradicts existing tradition, but is justified by obtained results. Four existing

wind forcing terms has been checked : *ZRP*, Chalikov, Xiao-Shemdin an Snyder ones. The only S_{in} term in the power form was *ZRP* forcing term, and only this corresponding experiment showed good agreement with the field experiments, for which p=1 and q=0.3. The other S_{in} terms lead to the Eq.(13), (14) for which indices p and q are the functions of dimensionless fetch. It is important to note that the magic relation Eq. (15) still holds for them too, which means that the corresponding spectra exhibit "local" self-similarity.

The most far-outlying from the reality results exhibits the numerical experiment performed with Snyder forcing, which happens to be sharply exceeding the reality. Presumably, this fact was realized even before [R21], and was the reason for long-wave dissipation inclusion into the model. This idea materialized in the form of *WAM*3 model, which had Snyder wind forcing term and long-wave dissipation as well. Apparently, *WAM*3 model numerical testing with exact expression for S_{nl} was never performed before the tests presented in current report.

The numerical test results presented below show that *WAM*3 model predicts too low levels of waves. It is satisfactory in only one aspect - it passes the ω^{-4} test explained in Section 4.

The obtained results can be estimated as successful start. The further perspectives are discussed in the **Conclusion**.

1.1 Current state of wind input source terms

Nowadays, the number of existing models of S_{in} is large, but neither of them has firm theoretical justification. Different theoretical approaches argue with each other. Detailed description of this discussion can be found in the monographs [R4], [R5] and the papers [R22], [R23], [R24], [R25] and [R26].

The development of wind waves models has begun as far as 1920-ies of the last century in the well-known works of Jeffreys [R27], [R28]. His model is semi-empiric and includes unknown "sheltering coefficient". All other existing theoretical models are also semi-empiric, with one exclusion – famous Miles model [R26]. This model is rigorous, but is related to idealized situation – initial stage of waves excitation by laminar wind with specific wind profile $U(z)$.

Miles theory application is hampered by two circumstances. First is the fact that atmospheric boundary layer is turbulent one, and creation of rigorous analytical theory of such turbulence is nowadays unsolvable problem.

There is the opinion, however, that wind speed turbulent pulsations are small with respect to horizontal velocity $U(z)$ [R29,R30,R31,R32], and in the first approximation they should be neglected [R30,R32]. This does not mean that turbulence is not taken into account at all. It is suggested that the role of the turbulence consists in formation of the averaged horizontal velocity profile.

The widely spread opinion is that horizontal velocity profile is distributed by logarithmic law

$$U(z) = 2.5u_* \ln\frac{z}{z_0} \tag{17}$$

Here u_* is friction velocity and z_0 – the roughness parameter

$$z_0 = C_{ch}\frac{u_*}{g} \tag{18}$$

where $C_{ch} \approx 3\cdot 10^{-2}$ is experimental dimensionless Charnock constant.

One should note that appearance of anomalously small constants, not having "formal justification", is extremely rare phenomenon in physics. Eq. (17), (18) mean that roughness parameter is very small: for typical ocean conditions – wind speed 10 m/sec on the height z=10 m we have $z_0 \approx 5\cdot 10^{-4} m$. Such roughness is only twice the size of viscid layer, defined from multiple experiments on turbulent wind flow over smooth metal plates.

Usage of Eqs. (17), (18) assumes therefore that ocean behaves as smooth metal surface. This is not correct. Horizontal momentum is transferred to the smooth plate on its surface itself, while in the ocean this process happens differently.

Momentum offtake from atmospheric boundary layer is smoothly distributed over the whole width of the boundary layer and begins from the highest "concurrence layer", i.e. from the height where phase speed of the fastest wave matches the horizontal velocity. Momentum offtake leads to horizontal velocity distribution $U(z)$ dependence on time, waves development level and energy spectrum.

Meanwhile, Miles instability increment is extremely sensitive to the horizontal velocity profile (there is no waves excitation for linear profile $U(z)$ in Miles theory, for example). The velocity profile is especially important for slight elevations of the order of several centimeters over the water surface, which is almost unknown and difficult for experimental measurements. However, there are some advances in this direction [R33,R29].

The necessity of taking into account the waves feedback into the horizontal velocity profile has been understood long time ago in the works of Fabricant [R30] and Nikolaeva, Zymring [R31]. It was later continued in the works of Jannsen [R32] and explained in details in the monograph [R5] in the form of "quasi-laminar" theory. This theory is not accomplished yet.

To consider the theory as self-consistent even in the approximation of turbulence absence, it is necessary to solve equations describing horizontal velocity profile $U(z)$ together with Hasselmann equation, describing energy spectrum evolution. This is not done yet either.

Aside that fact, many theoreticians do not share the opinion about turbulent pulsations insignificance, and consider them as the leading factor. Corresponding *TBH* theory by Townsend, Belcher and Hunt [R22] is alternative to quasi-laminar theory. Both theories are discussed in **[Error! Reference source not found.]**.

There is another approach, not connected with experimental analysis - numerical simulation of boundary atmospheric layer in the frame of empiric theories of turbulence. It was developed in the works [R23,R24,R25,R35]. Since those theories are insufficiently substantiated, the same relates to correspondingly derived wind input terms.

For all the variety of theoretical approaches of S_{in} definitions, all of them are "quasi-linear" [R20], where standard relation

$$\gamma(\omega,\theta)=\frac{\rho_a}{\rho_w}\omega\beta\left(\frac{\omega}{\omega_p},\theta\right) \tag{19}$$

is being used. Here $\omega_p=\frac{g}{u}$ where u is the wind speed, defined differently in individual models. Function β is dimensionless and is growing with the growth of $\frac{\omega}{\omega_p}$. However, even for the models exhibiting the most strong wind input, the value of β does not exceed several units and usually $0 < \beta < 1$. In some models (see, for example [R25]) β becomes negative for the waves propagating faster than the wind, or under large angle with respect to the wind.

Looking at multiple attempts of S_{in} experimental definition, one should note that all of them should be carefully critically analyzed. That criticism is not about the integrity of measurements itself, but about the used methodology and data interpretation correctness and the possibility of transfer of the conclusions made in artificially created environment to real ocean conditions.

Significant amount of the experiments, belonging to so-called "fractional growth method" category, has been performed through energy spectrum measurement in time and calculation of the corresponding γ through

$$\gamma=\frac{1}{\varepsilon(\omega,\theta)}\frac{\partial\varepsilon(\omega,\theta)}{\partial t} \tag{20}$$

Eq. (20) is, in fact, the linear part, or just two terms of the *HE* Eq. (1).

This method is intrinsically wrong, since it assumes that either advection $\frac{\partial\omega_k}{\partial\vec{k}}\frac{\partial\varepsilon}{\partial\vec{r}}$, or nonlinear S_{nl} terms of Eq.(1) are absent altogether, or relation

$$\frac{\partial\omega_k}{\partial\vec{k}}\frac{\partial\varepsilon}{\partial\vec{r}}=S_{nl} \tag{21}$$

is fulfilled.

First assumption is simply not correct, since neglected terms are defining in ocean conditions. The second assumption is almost fulfilled indeed, since the sea obeys *WTT*. But the terms in Eq.(21) are large, while the terms in Eq.(21) are relatively small. Thus there is no reason to neglect the terms Eq. (21).

In the relation to the "fractional growth method" we are just citing the single relevant publication by Plant [R36] where, it seems, author well understood the scarcity of this approach.

As a matter of fact, the real interest presents the experiments, which used measurements of the correlation between the speed of the surface growth and the pressure on the surface:

$$Q(\omega) = \mathrm{Re} < \eta(\omega) P^*(\omega) > \tag{22}$$

Unfortunately, the number of such experiments is limited, and not all of them have significant value for ocean phenomena description. Also, one should take out of consideration the experiments performed in laboratory conditions.

Consider, for example, the set of experiments described in [R37]. These experiments were performed in the wave tank of 40 *m* length and 1 *m* depth. The wind was blowing at the speed up to 16 *m/sec*, but they studied only short waves no longer than 3 *m*, moving no faster than 1.3 *m/sec*. Therefore, they studied the very short-wave tail of the function β in the conditions far from the ocean ones. The value of these measurements is not significant.

The same arguments relate to multiple and precisely performed measurements in the Lake George, Australia [R38]. The depth of this lake, in average, is about 1 *m*. That is why the waves not faster than 3.3 *m/sec* can propagate on its surface. The typical wind speed, corresponding to these measurements was 8-12 *m/sec*.

Therefore, while the results of these measurements are quite interesting, obtained expression for S_{in} is arguable not only because of non-improvement to "quasi-linear" theory, but also being in complete contradiction with it.

The quasilinear theory predicts smoothing of the velocity profile $U(z)$ with waves development. The wind input growth rate, however, was increasing with the wave level in the experiments [R39].

After critical analysis of experiments on S_{in} measurements, only three of them deserve an attention. Those are the experiments by Snyder et al. [R40], Hsiao, Shemdin [R41] and Hasselmann, Bosenberg [R42]. These experiments were performed in the open ocean and measured direct correlations of surface speed change and the pressure. Their accuracy was not quite high and scatter of data was significant, presumably, due to their contemporary technologies. Therefore, their interpretation is quite ambiguous. Anyhow, these experiments produced two well-known formulas for β. Next, we present β expressions for the cases analyzed in current report.

For Snyder et al. [R40] and Hasselman-Bosenberg [R42] cases

$$\beta = \begin{cases} 0.24(\zeta - 1) & for\ \zeta \geq 1 \\ 0, & for\ \zeta < 1 \end{cases} \tag{23}$$

For Hsiao-Shemdin [R41] case

$$\beta = \begin{cases} 0.12(\zeta - 1)^2 & for \ \ \zeta \geq 1 \\ 0, & for \ \ \zeta < 1 \end{cases} \tag{24}$$

For *ZRP* [**Error! Reference source not found.**] case

$$\beta = \begin{cases} 0.12(\zeta - 1)^2 & for \ \ \zeta \geq 1 \\ 0, & for \ \ \zeta < 1 \end{cases} \tag{25}$$

The difference between various S_{in} corresponding to Eq. (23)-(25) is significant. As it was shown before for wind forcing on measured spectra [R16], Snyder-Hasselmann-Bosenberg form gives 5-6 times bigger value of S_{in} than Hsiao-Shemdin one. Furthermore, the Hsiao-Shemdin form agrees with Jeffreys theoretical model, while Snyder-Hasselmann-Bosenberg one is not supported by any known theoretical models.

Fig.1 presents one-dimensional plots of four functions $\beta(\zeta)$ studied in numerical experiments presented below. We intentionally did not include lengthy Chalikov formula for corresponding $\beta(\zeta)$ for the sake of space saving purposes. Curious reader can find it in [R35].

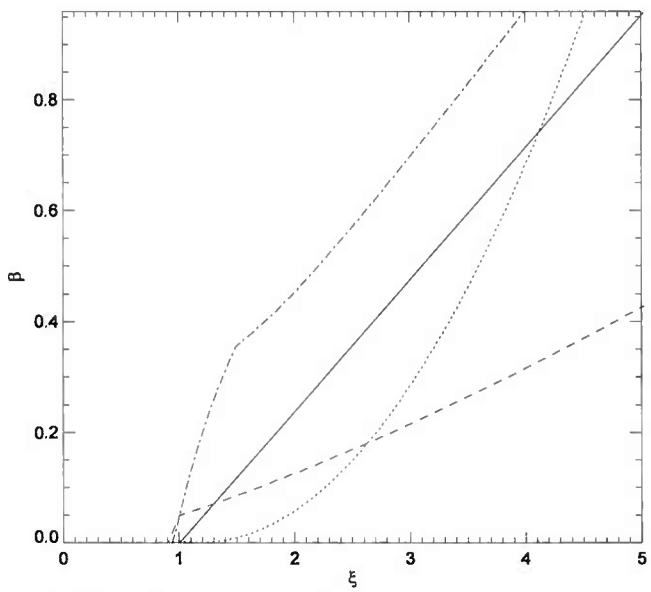

Figure 1 Four cases of function $\beta(\zeta)$ used in numerical experiments along the wind $\theta = 0$. Solid line: Snyder-Hasselmann-Bosenberg case Eq.(23); dashed line: Hsiao-Shemdin case Eq.(24), dashed-dotted line: Chalikov case [R35] and dotted line: ZRP case Eq. (25).

Summing up, we can conclude that at the moment there is no solid parameterization of S_{in} accepted by worldwide oceanographic community. Keeping that fact in a mind, we decided to go our own way – not to build new theoretical models and not to reconsider both old and completely new measurements of S_{in}.

For 68 years, counting from works of Sverdrup and Munk [R13], physical oceanography assimilated tremendous amount of wind-wave experimental data - wave energy and spectral peak frequency as the functions of limited fetch. Such experiments are analyzed in works [R16,R17,R18,R19]. From the

other side, numerical methods for solution of *HE* Eq. (1) with exact S_{nl} term have been improved significantly for duration-limited and fetch-limited domaina as well.

Therefore, we proposed purely new pragmatic approach to definition of S_{in}. We have chosen S_{in} function in a way that numerical solution of Hasselmann equation explains maximum amount of known field experiments. The result was the S_{in} function described in details in [**Error! Reference source not found.**] and named thereafter *ZRP* function.

It is important to emphasize that work [R1] assumed localization of energy dissipation in short waves. This assumption contradicts widely accepted concept, but we explain the difference in the following chapter.

1.2 Two scenarios of wave-breaking dissipation term: spectral peak or high-frequency domination?

In current section we explain why there is no need to use dissipation in the spectral peak area.

The spectral peak frequency damping is widely accepted practice, and is included as an option in the operational models *WAM*, *SWAN* and *WW*3. Historically, it was done apparently not for physical reasons, but by need for matching *HE* simulation results to the field experimental data.

This necessity was caused by wind input function S_{in} in Snyder form [R21,R43]. Too fast wave energy growth was observed in no-dissipation calculations, which didn't match the results of field measurements. Despite the results were obtained with the help of *DIA* substitute of S_{nl}, it is qualitatively correct, since it is also confirmed by presented below numerical calculations, which used exact nonlinear interaction term S_{nl}.

It is shown below that Snyder wind input without long-wave dissipation gives 5-6 times bigger energy growth than other tested wind input functions (*ZRP*, Chalikov and Hsiao-Shemdin). This doesn't mean, indeed, that long-wave dissipation exists. The necessity of its introduction is explained by Snyder model imperfection, based on not quite accurate experiments.

There are no physical reasons for energy-containing long waves breakings. Their steepness in the conditions of typically developed wave turbulence is not big: $\mu = <\nabla\eta^2>^{1/2} \sim 0.1$, or even smaller. Because this value is very far from limiting steepness of Stokes wave $\mu_S \approx 0.3$, these waves are essentially weakly-nonlinear. Besides those waves, shorter waves inevitably develop, having the steepness approaching to the critical one, and those waves break. There is, nevertheless, no reason to expect that these waves have the same phase velocity as the energy-containing ones.

Unfortunately, the theory of "wave-breakers" is not developed yet. In our view, which we don't consider based enough, one of the possible variants of such theory could be the following.

The primordial Euler equations for potential flow of deep fluid with free surface has the self-similar solution

$$\eta(x,t) = gt^2 F\left(\frac{x}{gt^2}\right) \tag{26}$$

This solution was studied numerically in the framework of simplified *MMT* (Maida-McLaughlin-Tabak) model of Euler equations [R44].

In Fourier space this solution describes the propagation to high wave-numbers and returning back to dominant wave spectral peak of fat spectral energy tail, corresponding in real space to sharp wedge formation at time t=0 and space point x=0. This solution describes formation of the "breaker".

In the absence of dissipation, this event is invertible in time. Presence of high-frequency dissipation "chops off" the end of the tail, just like "cigar cutter", and violates the tail invertability. Low and high harmonics, however, are strongly coupled in this event due to strong nonlinear non-local interaction, and deformed high wave-numbers tail almost immediately returns to the area of spectral peak. As soon as fat spectral tail return to the spectral peak area, total energy in the spectrum diminishes, causing settling of the spectral peak at lower level of energy. This process of "shooting" of the spectral tail toward high wave-numbers, and its returning back due to wave breaking is the real reason of "sagging down" of the energy profile in the spectral peak area, but was erroneously associated with the presence of the damping in the spectral peak area. This explanation shows that individual wave-breakings studies [R39,R45] are not the proof of spectral peak damping presence.

Also there is another, direct proof of the fact that the damping is localized in the area of short waves. It is the measurements of quasi-one-dimensional "breakers" speed propagation – strips of foam, which accompany any developed wave turbulence. Those experiments, recently performed by P. Hwang and his team [R46,R47,R48,R49], show that wave breakers propagate 4-5 times slower than the crests of leading waves.

Slowness of the breakers means that their characteristic sizes are several times smaller than energy-containing waves. Thus, "wave-breaking" is the phenomenon occurring in the short scales region. Of course, the short waves are modulated by the long ones, which amplifies the "wave-breaking" process. Presentation of that process as direct energy offtake from long waves is not confirmed, however, neither by experimental observations, nor analytical analysis.

Nevertheless, operational wind waves predicting models routinely use empirical expressions for wind-wave dissipation due to wave-breaking. The corresponding dissipation term in original notations is given by [50]

$$S_{diss}(k,\theta) = C_{ds}\hat{\sigma}\frac{k}{\hat{k}}\left(\frac{\alpha}{\hat{\alpha}_{PM}}\right)N(k,\theta) \tag{27}$$

$$\hat{\sigma} = \left(\overline{\sigma^{-1}}\right)^{-1} \tag{28}$$

$$\hat{\alpha} = E\hat{\sigma}^{-2}g^{-2} \tag{29}$$

where $N(k,\theta)$ is the wave action spectrum, σ is the frequency, k is the wavenumber, θ is the angle, E is the total energy, $C_{ds} = -2.36\cdot 10^{-5}$, $\alpha_{PM} = 3.02\cdot 10^{-3}$ is the value of $\hat{\alpha}$ for PM spectrum.

This formula assumes that dissipation is concentrated in the long-waves region and numerical experiments, presented in Section 9, show that it is realized that way, see Fig.32. This mean that Eqs. (27)-(29) are not confirmed by performed ZRP numerical simulation.

Currently, the set of experiments on direct numerical solution of the primordial dynamical Euler equations is carried out, based both on exact [R51] and approximate [R52] equations using small wave slope parameter expansions as well. Part of the results are already published [R51]. They shows that the dissipation due to wave-breaking of the small-slope waves is, at least, by the order of magnitude smaller than used in the operational models *WAM*3 and *SWAN*. More detailed results will be published soon in [R52].

Thus, it is reasonable to suppose that wave-breaking dissipation is localized in short scales. The population of waves having frequencies 3-4 times bigger than spectral maximum frequency is called "Phillips sea" [R53,R54]. The "Phillips sea" contains no more than 2% of the total wave energy, but the whole energy dissipation fueled by energy flux from long waves is happening right in that place. It is proved experimentally that "Phillips sea is described by universal Phillips spectrum $\varepsilon \approx \frac{\alpha g^2}{\omega^5}$, where $\alpha \approx 0.01$ is dimensionless constant, while for Pierson - Moscowitz spectrum $\alpha = 0.081$ [R55] .

"Phillips sea" is quite interesting physical object. It contains breakers of different statistically uniformly distributed sizes [55] down to capillary ones $\lambda \approx 1.7\, cm$. Exact form of "Phillips sea" energy dissipation function is unknown. Recently, quite plausible model of such function has been presented in [R56], which is hoped to become the subject of oceanographic community discussion.

1.3 Numerical experiments set-up

The subject of numerical solution was stationary *HE* Eq.(7) for different wind input functions.

The total of 5 different wind inputs have been tested with one difference: the first 4 tests were done for simplified equation

$$\frac{\partial \omega_k}{\partial k}\frac{\partial \varepsilon}{\partial x} = S_{nl} + S_{in} \tag{30}$$

assuming absence of low-frequency dissipation and presence of the "implicit" high-frequency dissipation. The fifth test - *WAM*3 model - included besides short-wave "implicit" dissipation also long wave dissipation according to Eq.(27)-(29) in the frame of "full" version of stationary *HE* Eq.(7) .

All simulations were performed with help of *WRT* method [R9] previously used in [R8,R56-R64] on the grid of 71 point in frequency and 36 point in angle domains.

1.4 The details of "implicit" damping implementation

One should specifically stop on the details of the "implicit" high-frequency damping used in all five numerical simulations. The procedure of inclusion of the "implicit" damping consists in continuation

of the spectral tail by Phillips law $A(\omega_{crit})\cdot\omega^{-5}$, where $A(\omega_{crit})$ is dynamically changing in time constant.

The coefficient $A(\omega_{crit})$ in front of ω^{-5} is not exactly known, but is unnecessary to be defined in the explicit form - it is dynamically determined from the continuity condition of the spectrum at frequency ω_0 on every time step. In other words, starting point of the Phillips spectrum coincides with the last point of the dynamically changing spectrum at the frequency point $\omega_{crit}=2\pi f_{crit}$, where $f_{crit}\approx 1.1\,Hz$ as per Resio and Long experimental observations [R57,R58].

This is the way the high frequency "implicit" damping is incorporated into alternative computational framework of *HE*.

One should note that recently developed analytical model [R55] describes automatically the transition from *KZ* spectrum ω^{-4} to Phillips tail ω^{-5} [R56]. Such modification of the "implicit" damping is in the future plans, but the question of finer details of high-frequency "implicit" damping structure is of secondary importance at current stage of the alternative framework development.

1.5 *WTT* facts used in numerical simulation

As a rule, confirmed by field and numerical observations, the wave energy spectrum has sufficiently sharp peak at $\omega\approx\omega_p$. However, almost immediately after the spectral peak at $\omega\approx\omega_p$ the advection term $\frac{\partial\omega}{\partial k}\frac{\partial\varepsilon}{\partial x}$ becomes insignificant and the original stationary *HE* Eq.(7) is transformed into

$$S_{nl}+S_{in}+S_{diss}=0 \tag{31}$$

Comparison with Eq. (10) shows that Eq.(31) can be rewritten in the form

$$F(\omega,\theta)=\left(\Gamma(\omega,\theta)-\gamma(\omega,\theta)+\gamma_{diss}(\omega,\theta)\right)\cdot\varepsilon(\omega,\theta) \tag{32}$$

As it was shown in [R7,R20], nonlinear dissipation $\Gamma(\omega,\theta)$ in the "universal area" $\omega>1.5\omega_p$ is several times greater than wind forcing. Therefore, Eq. (31) can be rewritten in the first approximation as

$$S_{nl}=0 \tag{33}$$

This equation has the family of stationary solutions. The most simple and well-known is isotropic solution

$$\varepsilon(\omega,\theta)=\frac{C_p g^{4/3}}{\omega^4}P^{1/3}=\frac{\beta_{KZ}}{\omega^4} \tag{34}$$

Here P is the energy flux into the high wavenumbers region. Our experiments show that it changes in the limits $(2 \div 3) \cdot 10^{-6}\, m/\sec$. C_p is Kolmogorov constant, which value is now exactly known :

$$C_p = 4\pi \cdot 0.194 = 2.43 \tag{35}$$

From here one can estimate characteristic the value of β_{KZ}

$$\beta_{KZ} = C_p g^{4/3} P^{1/3} \approx 0.6\ \text{m/sec} \tag{36}$$

According to *WTT*, the value of β_{KZ} should be the constant in the region $1.5\omega_p < \omega < \omega_{crit}$. Here $\omega_{crit} = 2\pi \cdot 1.1 = 6.91$ is the critical frequency at which the "implicit" damping is turning on. The energy flux at this area is diminishing proportionally to ω^{-3}, and β_{KZ} is not the constant anymore - one has to substitute β_{KZ} by $\beta_{KZ} \cdot \frac{\omega_{crit}}{\omega}$.

Real energy spectrum in the universal area is not quite isotropic. Eq. (33) besides isotropic has exact anisotropic solutions as well [R???]. As far as concerns considered cases, the solutions do not differ too much from the isotropic ones. Detailed discussion of those circumstances is outside the scopes of current report.

Let's discuss self-similar solutions of the conservative *HE* Eq.(21). This equation has the family of self-similar solutions

$$\varepsilon = \zeta^{p+q} F(\omega \zeta^{q}) \tag{38}$$

where q and p are the constants, connected by the "magic relation"

$$10q - 2p = 1 \tag{39}$$

In this case the energy and frequency of the spectral maximum are the power functions

$$\varepsilon = \varepsilon_0 \cdot \zeta^{p} \tag{40}$$

$$\hat{\omega} = \omega_0 \cdot \zeta^{q} \tag{41}$$

Eq.(21) has the single self-similar solution only in the case when β from Eq.(19) (don't mix with β_{KZ} from Eq. (34))!) is power function of frequency:

$$\beta = \omega^{s} f(\theta) \tag{42}$$

Now the constant q is defined unambiguously as $q = \frac{1}{2+s}$ [R1].

As it was already mentioned, practically all ocean field experiments demonstrate power dependencies Eq. (40), (41). However, there is scattering in definition of the exponent p in the range $0.74 < p < 1.1$.

It's quite possible that this scattering is due to absence of universal expression for S_{in}, useful for any atmospheric boundary layer state.

The experiments of Kahma [R19] performed for "stable" and "unstable" atmosphere gave the different values of p. However, the "magic relation" Eq. (39) still holds true for those different cases [17]. This fact holds the promise that *WTT* always works.

More than the half of the experiments have the values $p = 1,\ q = 0.3$. Such self-similarity occurs if $s = 4/3$. This fact together with field experimental data [**Error! Reference source not found.**, **Error! Reference source not found.**] leads to the appearance of *ZRP* wind input term [R1].

1.6 Checking of the new modeling framework against theoretical predictions and field measurements

To check alternative framework for *HE* simulation, we performed numerical tests for waves excitation in limited fetch conditions. As it was already mentioned, alternative framework is based on exact nonlinear term S_{in} and *ZRP* new wind input term:

$$S_{in} = \gamma\varepsilon \tag{43}$$

$$\gamma = 0.05\frac{\rho_{air}}{\rho_{water}}\omega\left(\frac{\omega}{\omega_0}\right)^{4/3} f(\theta) \tag{44}$$

$$f(\theta) = \begin{cases} \cos^2\theta & for \quad -\pi/2 < \theta < \pi/2 \\ 0 & \text{otherwise} \end{cases} \tag{45}$$

$$\omega_0 = \frac{g}{u_{10}},\ \frac{\rho_{\text{air}}}{\rho_{\text{water}}} = 1.3\cdot 10^{-3} \tag{46}$$

Fig.2 shows total energy growing along the fetch by power law in accordance with Eq.(40) with p=1.0, see Fig.3.

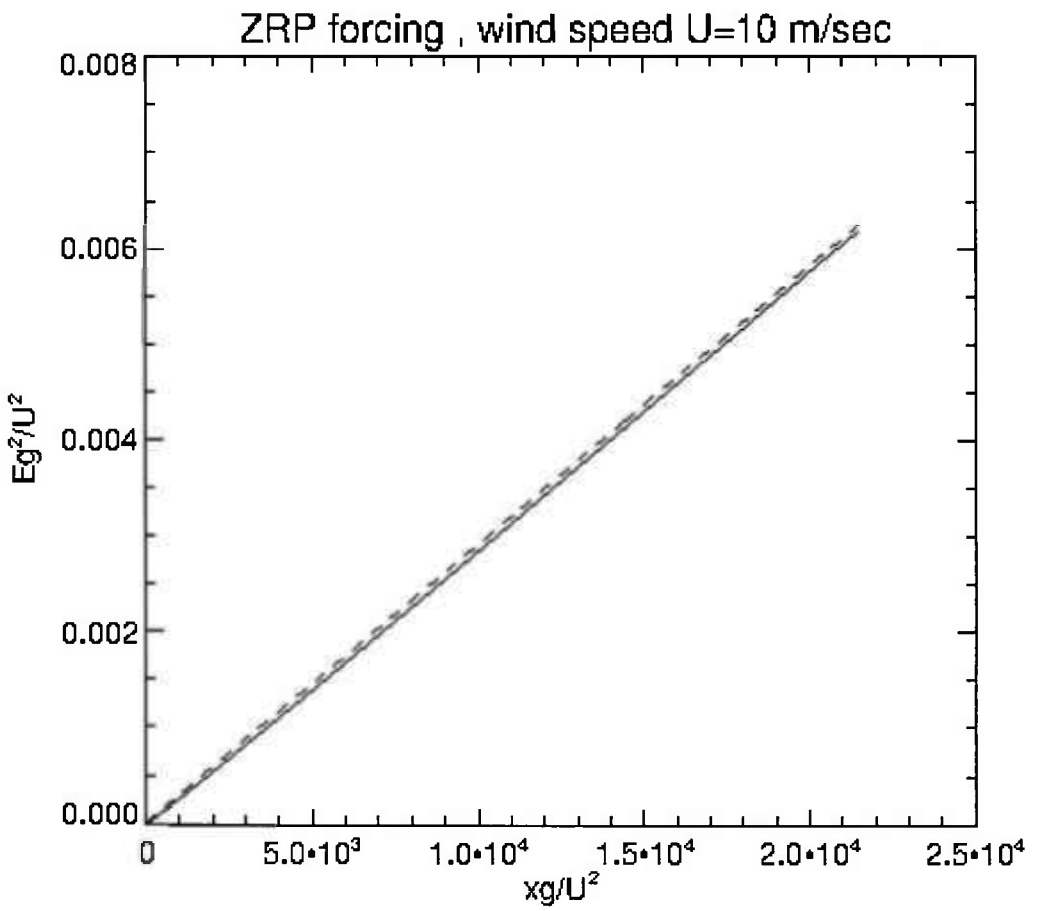

Figure 2 Dimensionless energy dependence on the dimensionless fetch in numerical experiment (solid line). Dashed line – fit by $2.9 \cdot 10^{-7} \cdot \frac{xg}{U^2}$

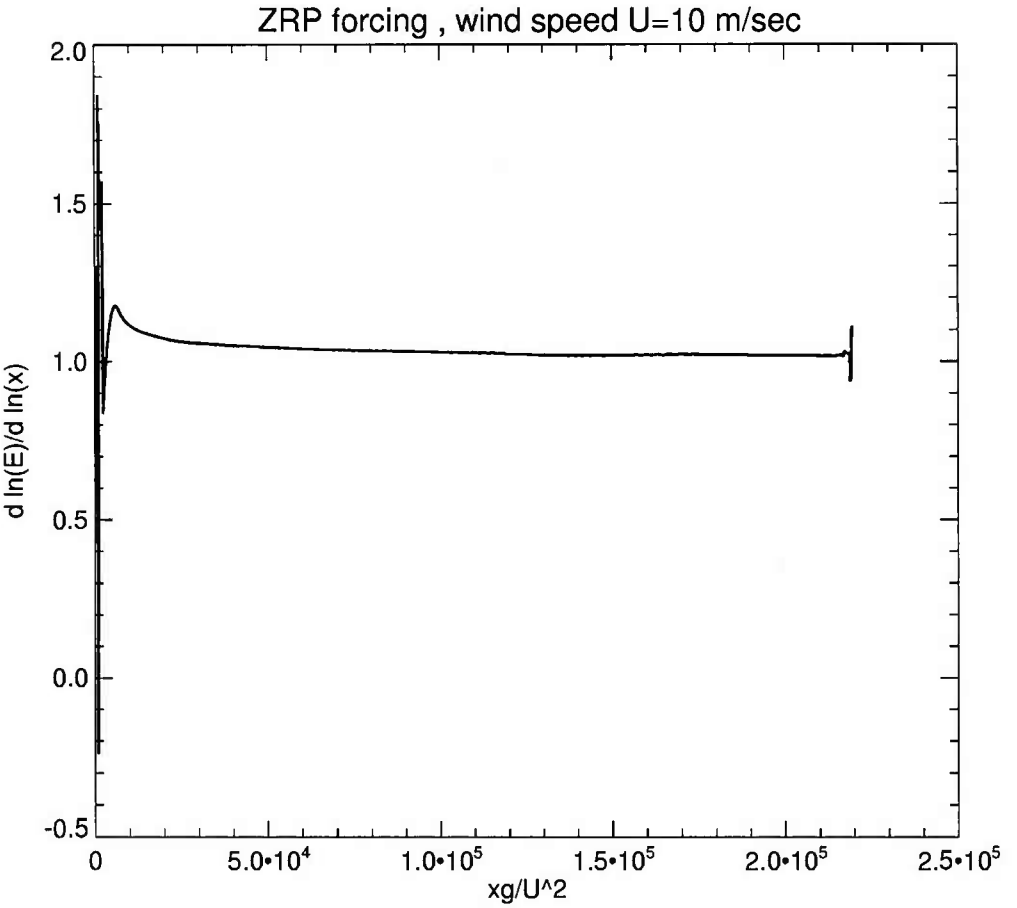

Figure 3 Exponent p of the energy growth as a function of dimensionless fetch.

Dependence of mean frequency on the fetch, shown on Fig.4, also demonstrates perfect correspondence of numerical results and corresponding self-similar dependence Eq.(41) with q=0.3, plotted on Fig.5. Because of good coincidence of mean and peak frequencies on Fig.4, the former is used in the following self-similarity analysis.

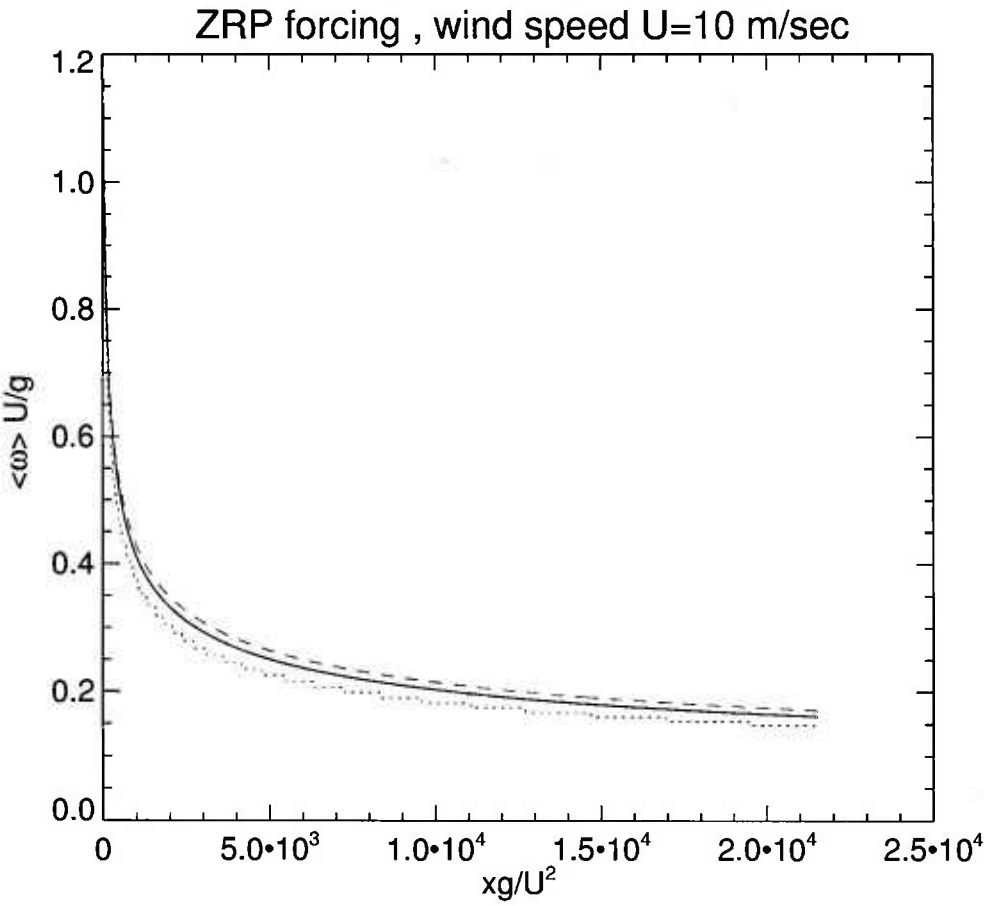

Fig.4 Dimensionless mean frequency as a function of dimensionless fetch (solid line) calculated as $<\omega>=\frac{\int \omega n d\omega d\theta}{\int n d\omega d\theta}$, **where** $n(\omega,\theta)$ **is the wave action spectrum; dotted line – peak frequency** ω_p, **dashed line – fit** $3.4\cdot\left(\frac{xg}{U^2}\right)^{-0.3}$

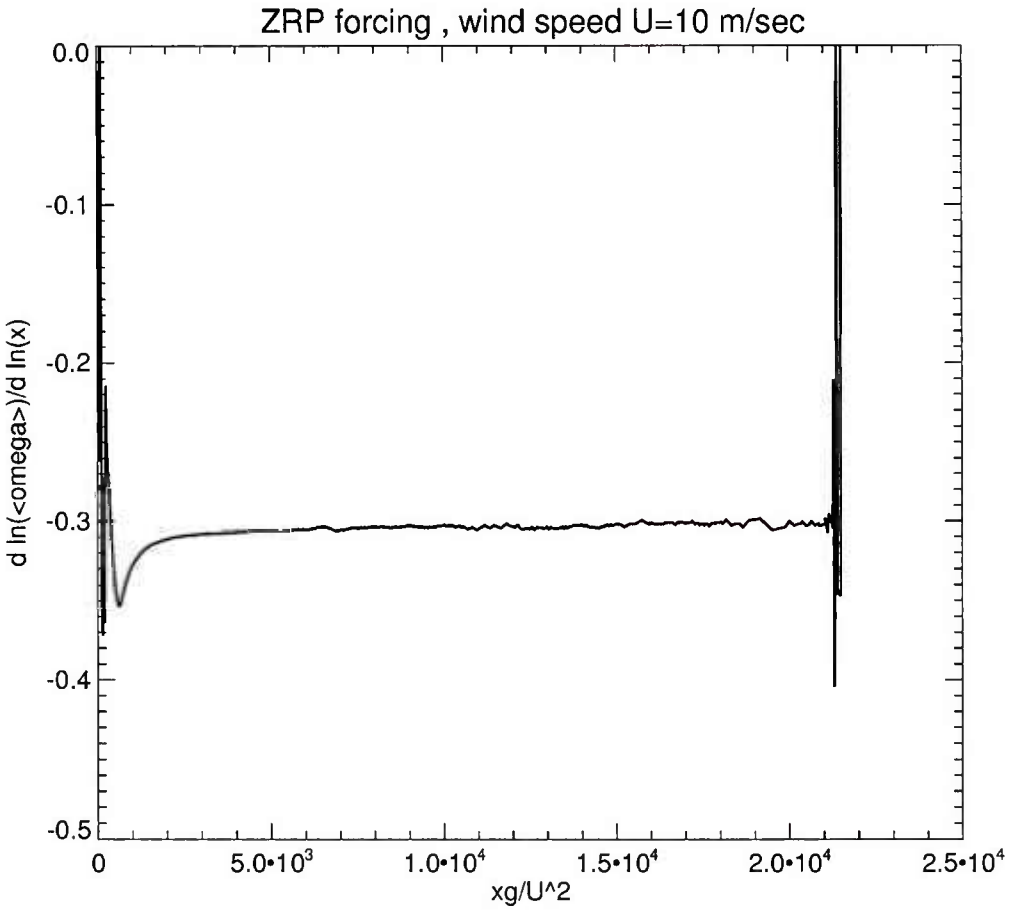

Fig.5 Exponent q of mean frequency as the function of dimensionless fetch.

Fig.6 presents directional spectrum as a function of frequency in logarithmic coordinates.

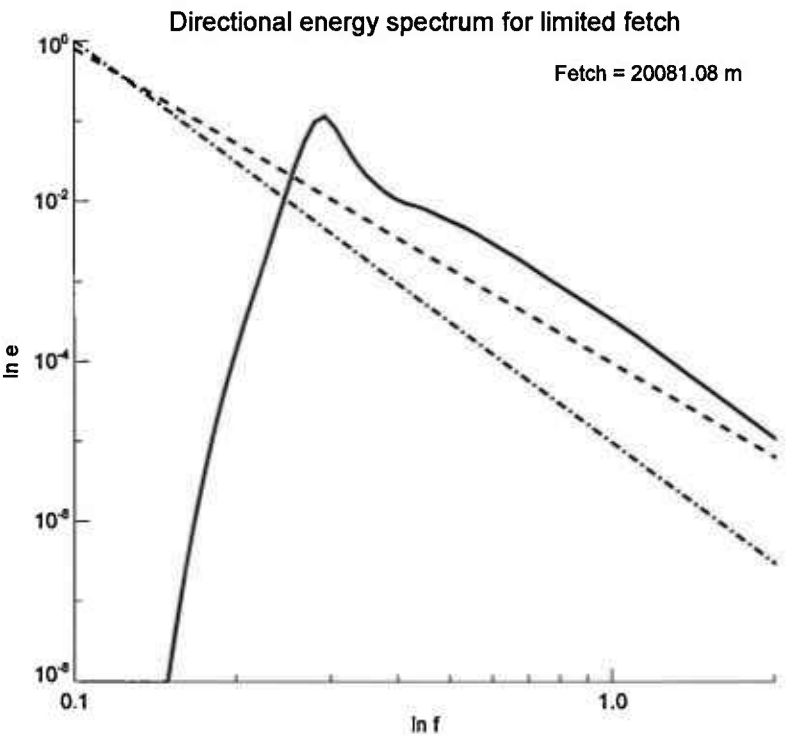

Fig.6 Logaithm of spectral energy density as a function of frequency logarithm (solid line). Dashed line – fit $\sim \omega^{-4}$; dash-dotted line – fit $\sim \omega^{-5}$.

One can see that energy curve on the left figure consists of segments of:

1. Spectral maximum area
2. Kolmogorov-Zakharov spectrum ω^{-4}
3. Phillips high frequency tail ω^{-5}

Fig.7 presents "magic relation" (10q-2p) as a function of fetch. It is in perfect accordance with self-similar prediction Eq. (39).

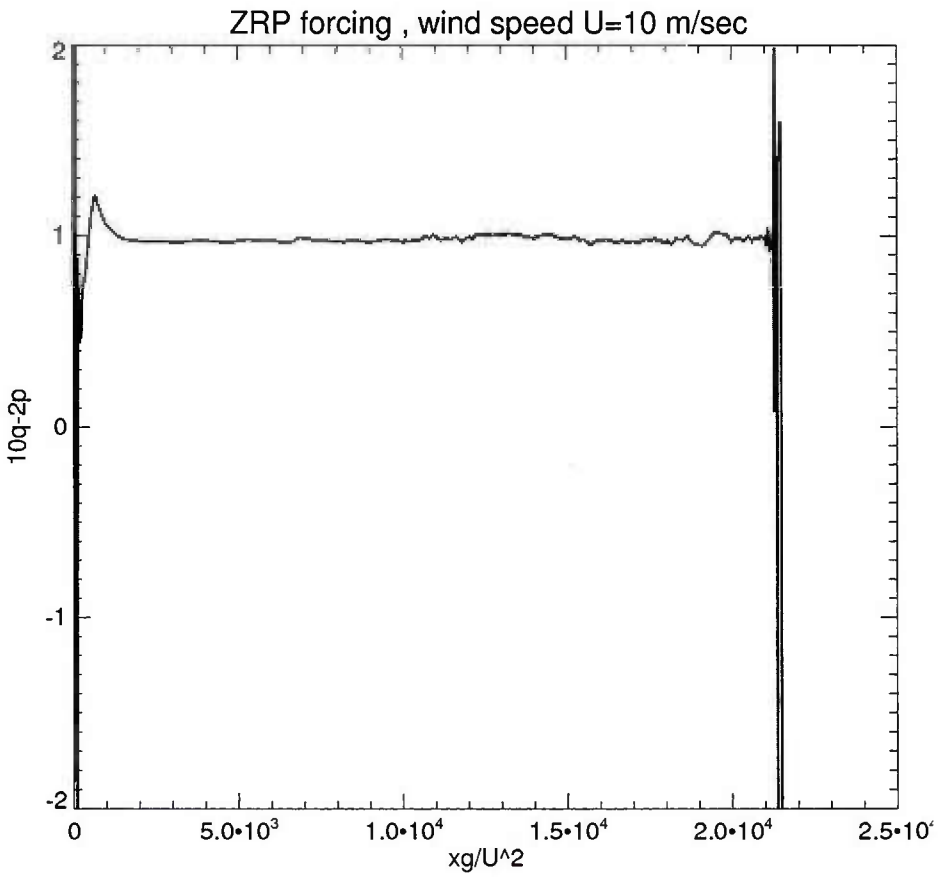

Figure 7: "Magic relation" (10q-2p) as a function of dimensionless fetch.

We conclude that alternative framework for *HE* simulation with *ZRP* wind input term reproduces the following analytical features of *HE*:

1. Self-similar solutions with correct exponents
2. Kolmogorov-Zakharov spectra ω^{-4}

Table 1 presents results of calculation [R6] of the exponents p and q for 14 different experimental observations with the last row corresponding to limited fetch growth numerical experiment within alternative *ZRP* framework. One can see good correspondence between theoretical, experimental and numerical values of p and q.

Experiment	p	q
Babanin, Soloviev 1998	0.89	0.28
Walsh et al. (1989) US coast	1.0	0.29
Kahma, Calkoen (1992) unstable	0.94	0.28
Kahma, Pettersson (1994)	0.93	0.28
JONSWAP by Davidan (1980)	1.0	0.28
JONSWAP by Phillips (1977)	1.0	0.25
Kahma, Calkoen (1992) composite	0.9	0.27
Kahma (1981, 1986) rapid growth	1.0	0.33
Kahma (1986) average growth	1.0	0.33
Donelan *et al.* (1992) St Claire	1.0	0.33
Ross (1978), Atlantic, stable	1.1	0.27
Liu, Ross (1980), Lake Michigan, unstable	1.1	0.27
JONSWAP by Hasselmann et al. (1973)	1.0	0.33
Mitsuyasu et al. (1971)	1.0	0.33
ZRP numerics	1.0	0.3

Table 1 The results of calculation [R6] of the exponents p and q for 14 different experimental observations with the last row corresponding to limited fetch growth numerical experiment within alternative *ZRP* framework.

1.7 Tests for separation of trustworthy wind input terms from non-physical ones

As it was already discussed, there are plenty of historically developed parameterizations of wind input terms. Analysis of nonlinear properties of *HE* in the form of specific self-similar solutions and

Kolmogorov-Zakharov law for direct energy cascade allows proposing the set of tests, which would allow separation of physically justified wind-input terms S_{in} from non-physical ones:

1. Checking powers of observed energy and mean frequency dependencies along the fetch versus predicted by self-similar solutions.
2. Checking the "magic relations" Eq.(39) between exponents p and q for observed energy and frequency dependencies along the fetch.
3. Checking exponents of directional spectral energy dependencies versus Kolmogorov-Zakharov exponent -4

We applied such tests to the results of *HE* simulations which used the following popular wind input terms within alternative framework:

1. Chalikov S_{in} term [R35,R25]
2. Snyder S_{in} term [R40]
3. Hsiao-Shemdin S_{in} term [41]
4. *WAM3* S_{in} term [50]

Test of Chalikov wind input term

Fig.8 shows that total energy growth along the fetch significantly exceeds observed in *ZRP* simulation, and value of the corresponding exponent significantly deviates from theoretical value $p=1.0$, see Fig.9.

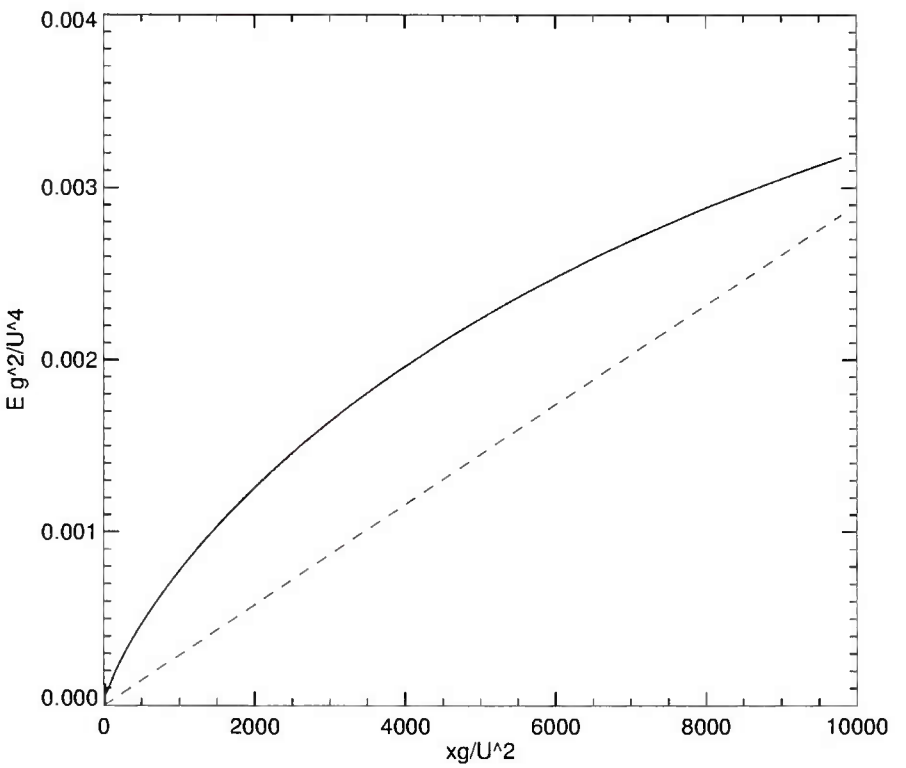

Fig.8 Same as Fig.2, but for Chalikov S_{in}

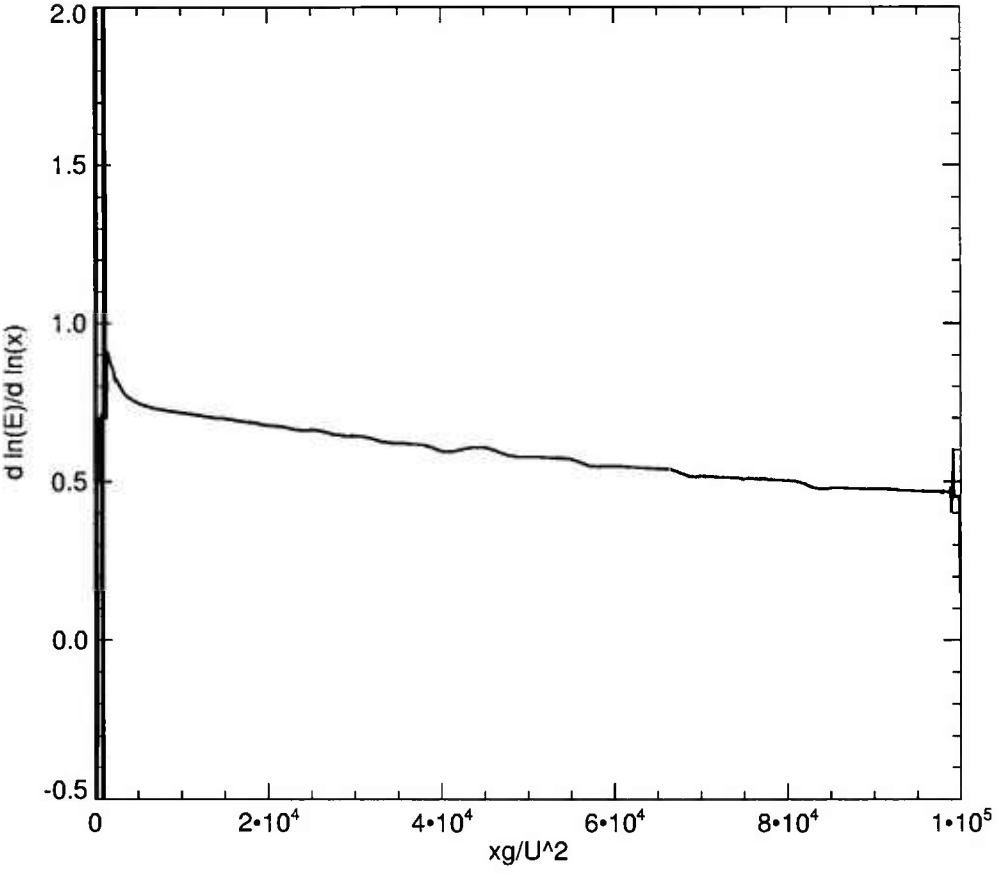

Fig.9 Same as Fig.3, but for Chalikov S_{in}

Dependence of mean frequency on the fetch, shown on Fig.10, also deviates from *ZRP* numerical results and corresponding self-similar exponent $q=0.3$, see Fig.11.

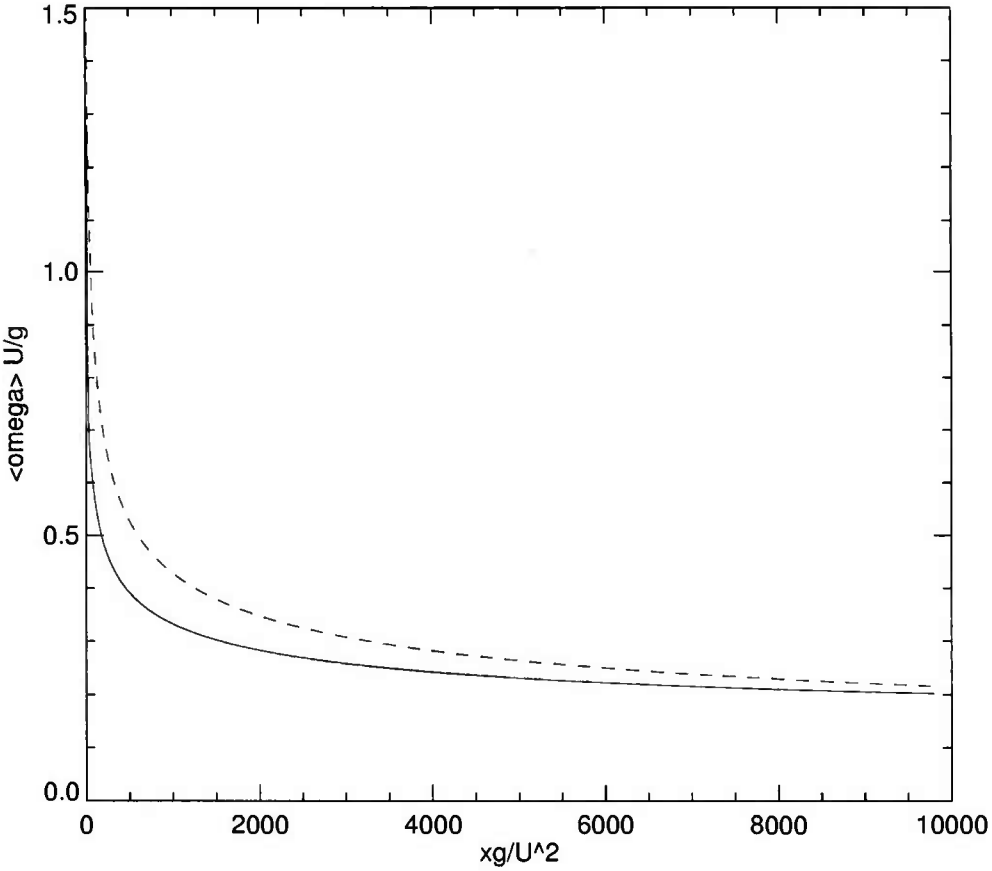

Fig.10 Same as Fig.3, but for Chalikov S_{in}

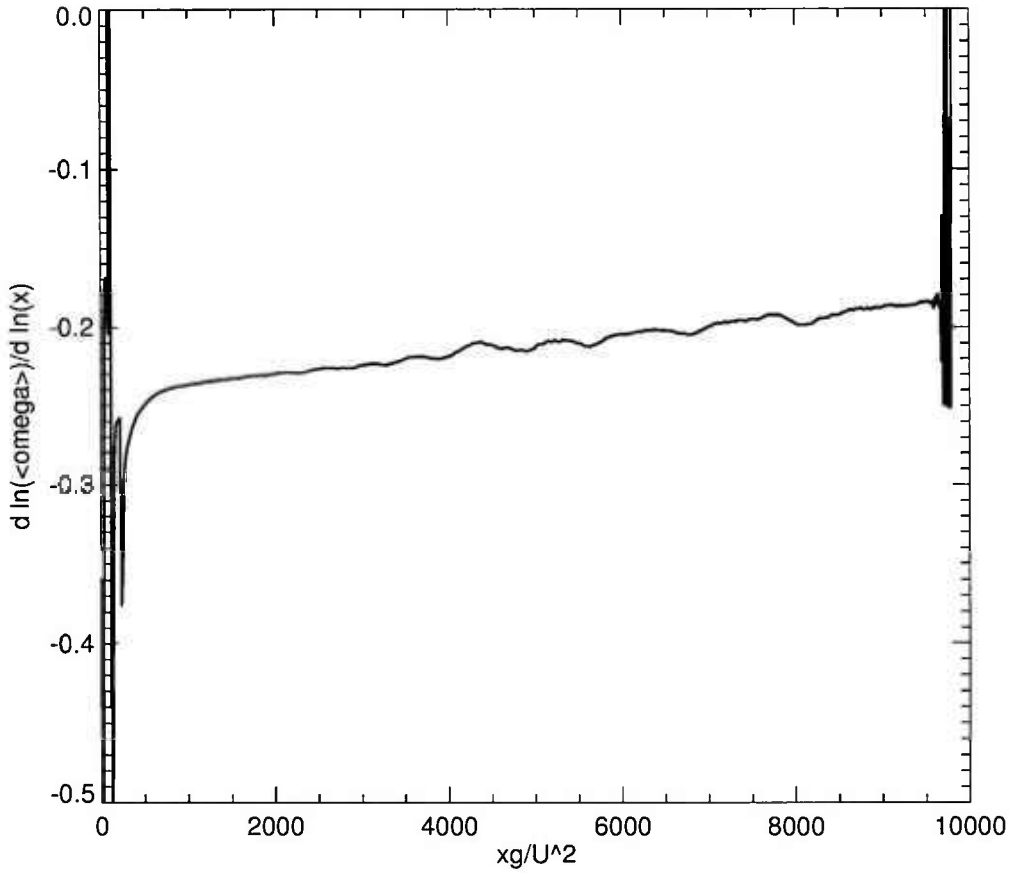

Fig.11 Same as Fig.4, but for Chalikov S_{in}

Fig.12 presents directional spectrum as a function of frequency in logarithmic coordinates. One can see that similar to *ZRP* case we observe:

1. Spectral maximum area
2. Kolmogorov-Zakharov spectrum ω^{-4}
3. Phillips high frequency tail ω^{-5}

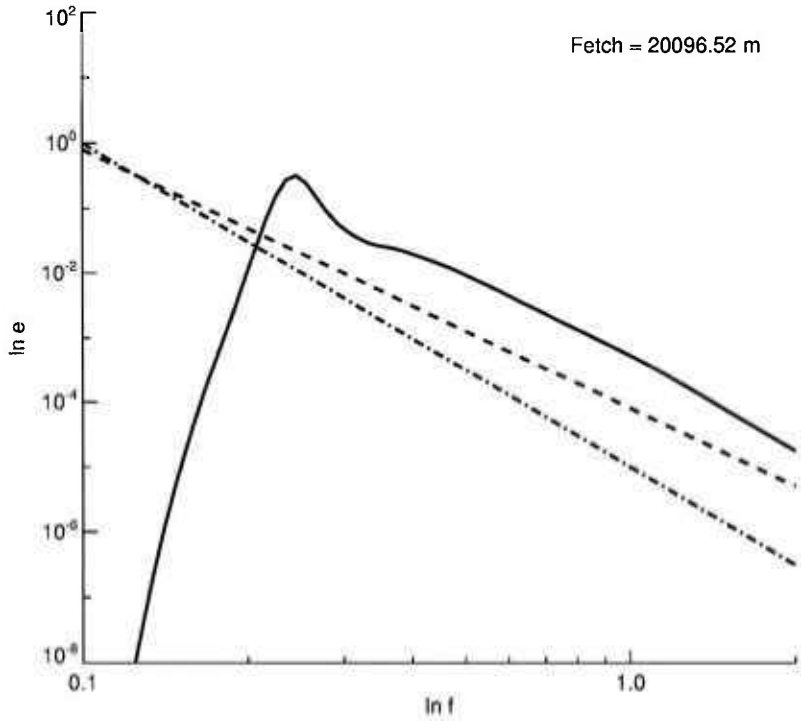

Fig.12 Same as Fig.5, but for Chalikov S_{in}

Fig.13 presents combination ($10q$-$2p$) as a function of the fetch. It is surprising that it is in perfect accordance with the "magic relation" Eq. (39). It mean that despite incorrect values p and q along the fetch, their combination ($10q$-$2p$) still holds in complete accordance with theoretical prediction, i.e. self-similarity is fulfilled locally.

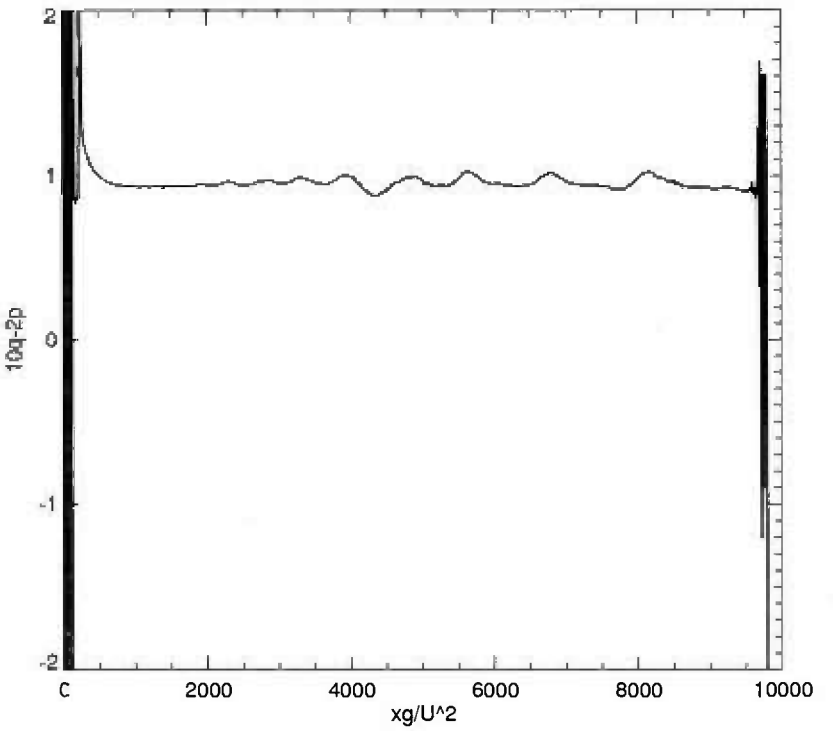

Figure 13: "Magic relation" (10*q*-2*p*) as a function of the fetch for Chalikov wind input term.

1.8 Test of Snyder wind input term

Fig.14 shows that total energy growth along the fetch significantly exceeds *ZRP* case, but has the value of the exponent close to $p=1.0$ versus the fetch, see Fig.15.

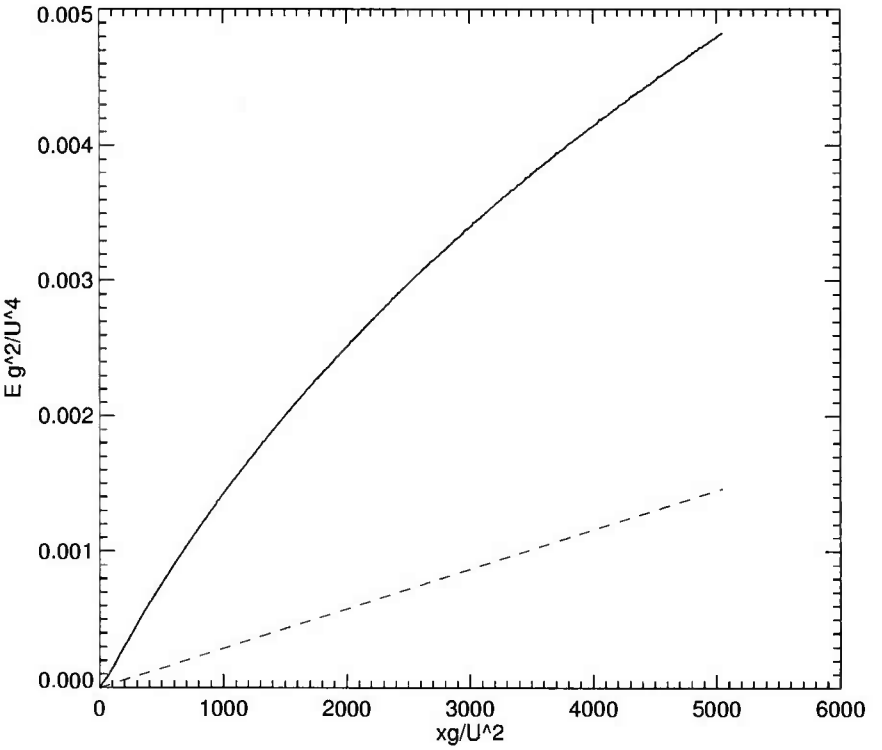

Fig.14 Same as Fig.2, but for Snyder S_{in}

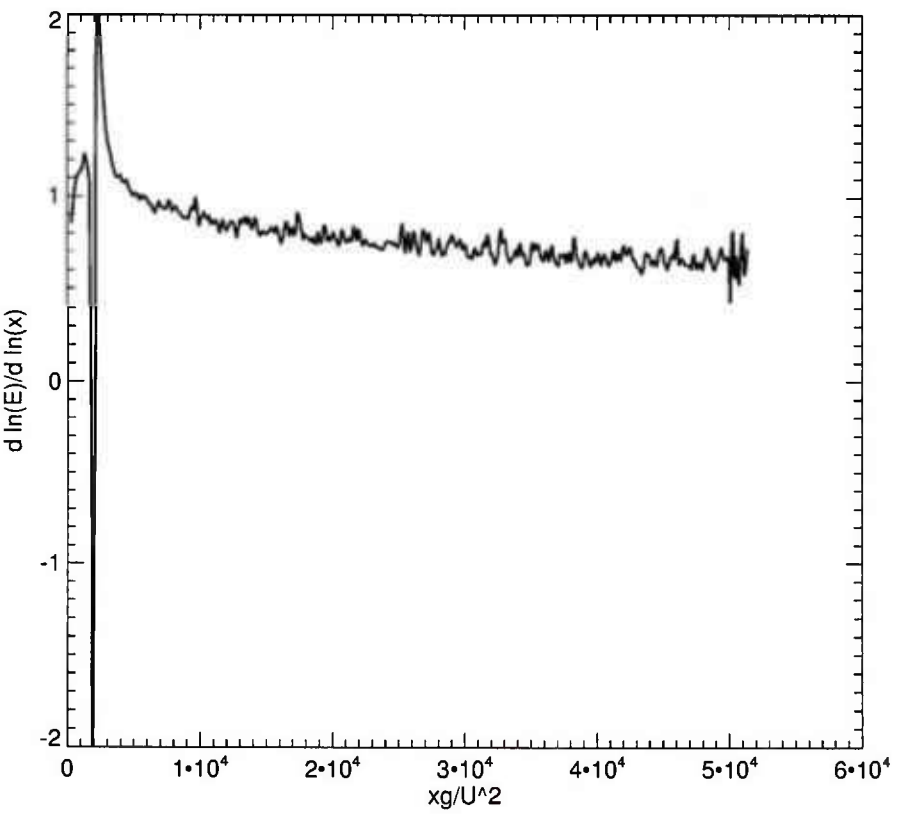

Fig.15 Same as Fig.3, but for Snyder S_{in}

Dependence of mean frequency against the fetch shown on Fig.16 is lower than *ZRP* numerical results, but has fairly close value to self-similar solution index q=0.3, see Fig.17.

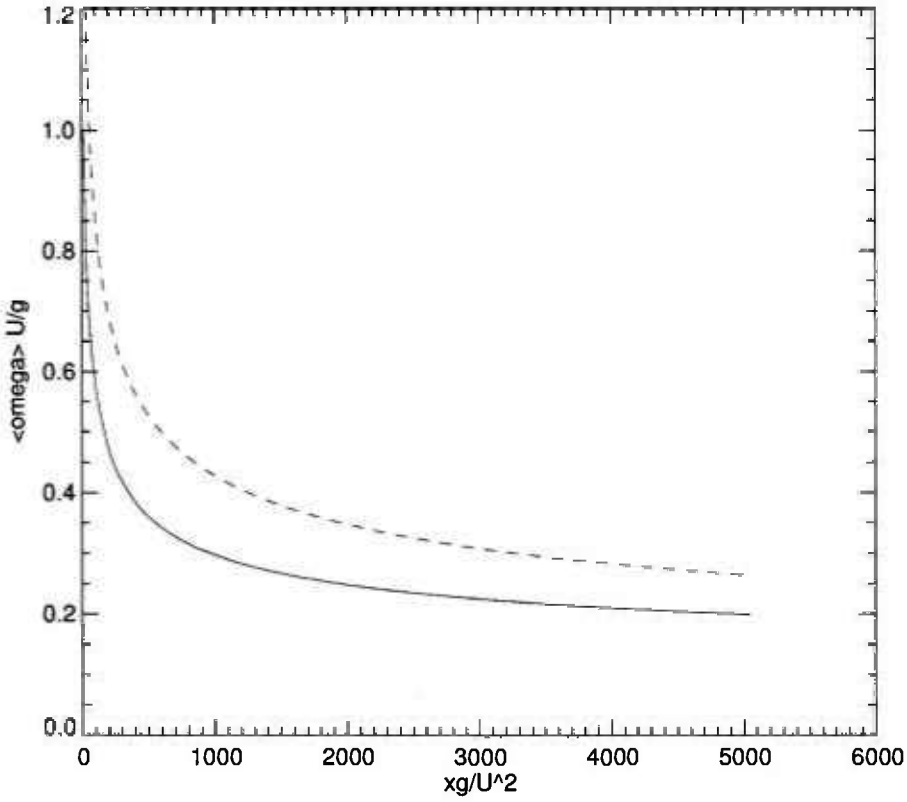

Fig.16 Same as Fig.4, but for Snyder S_{in}

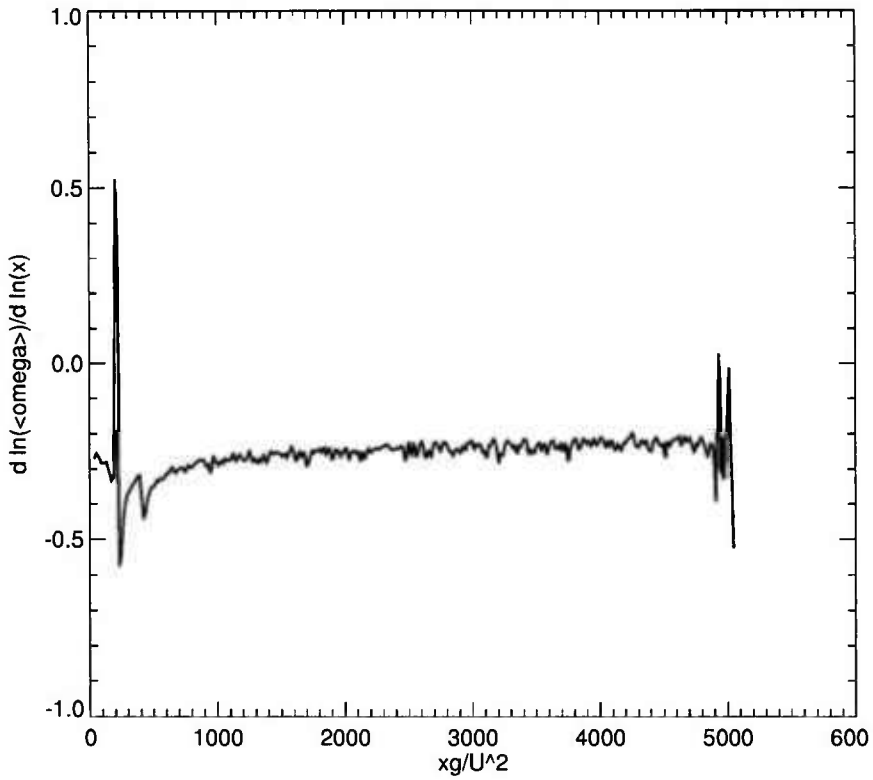

Fig.17 Same as Fig.5, but for Snyder S_{in}

Fig.18 presents directional spectrum as a function of frequency in logarithmic coordinates. One can see:

1. Spectral maximum area
2. Kolmogorov-Zakharov spectrum ω^{-4}
3. Phillips high frequency tail ω^{-5}

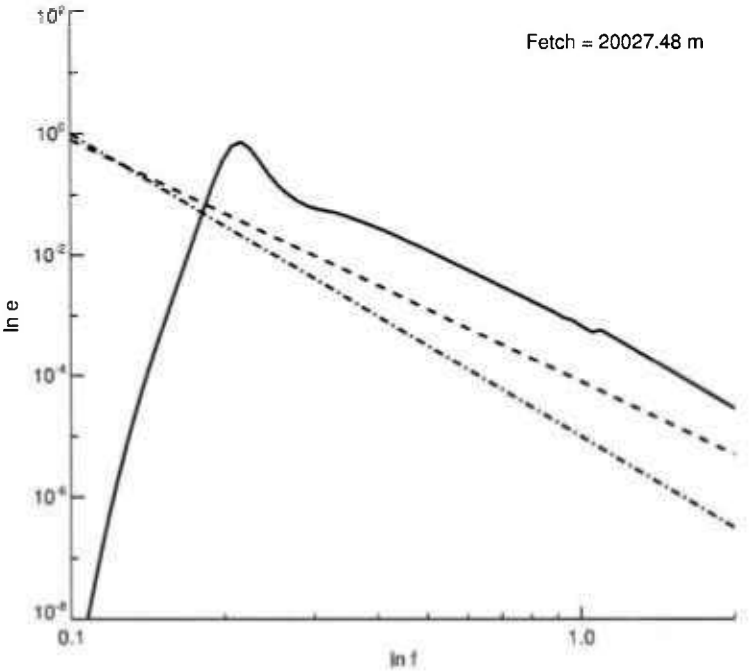

Fig.18 Same as Fig.6, but for Snyder S_{in}

Fig.19 presents the combination ($10q$-$2p$) as the function of the fetch. Again, it is in perfect accordance with the theoretical relation Eq. (39). As in Chalikov case it means that despite not perfect values of p and q and too fast energy growth along the fetch, their combination ($10q$-$2p$) still holds in complete accordance with theoretical prediction, i.e. self-similarity is also fulfilled locally in Snyder case.

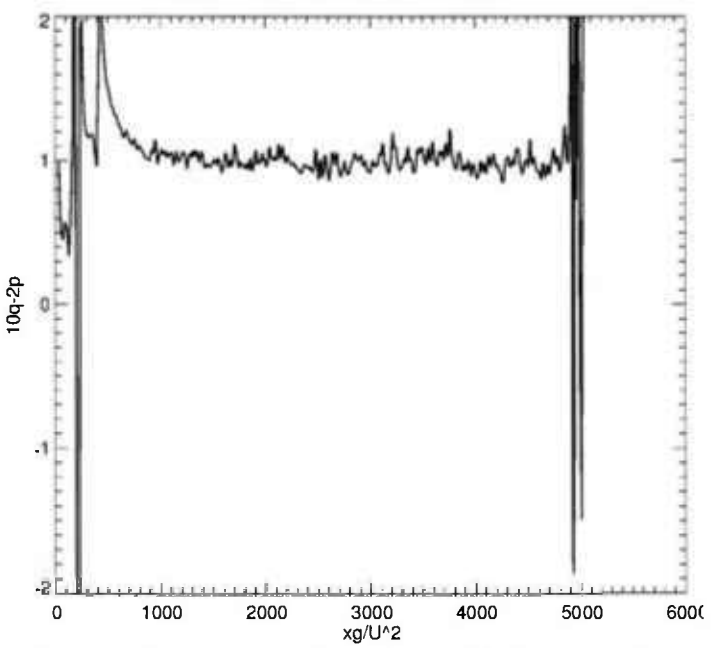

Figure 19 Relation ($10q$-$2p$) as a function of the fetch for Snyder wind input term.

1.9 Test of Hsiao-Shemdin wind input term

Fig.20 shows that total energy growth along the fetch strongly underestimates *ZRP* simulation, and has the asymptotic value of exponent p=0.5, see Fig.21

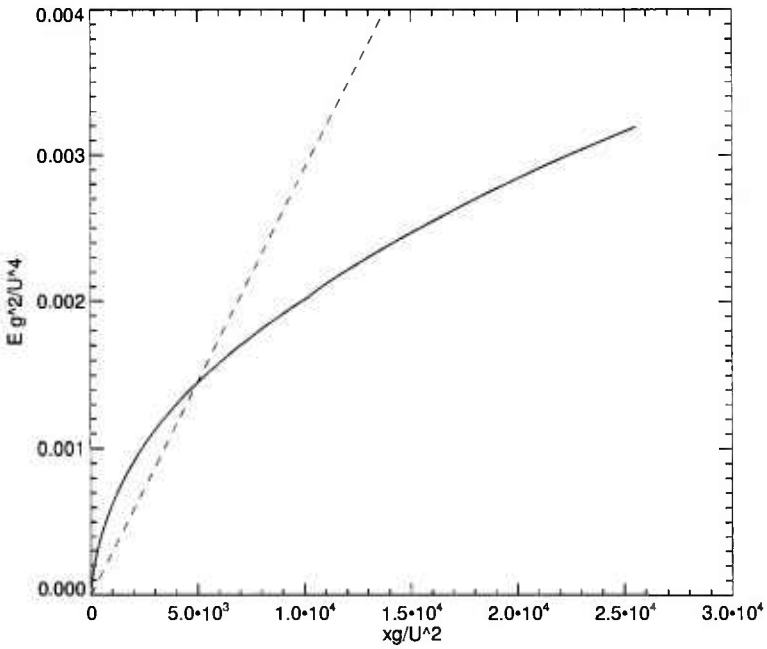

Fig.20 Same as Fig.2, but for Hsiao-Shemdin S_{in}

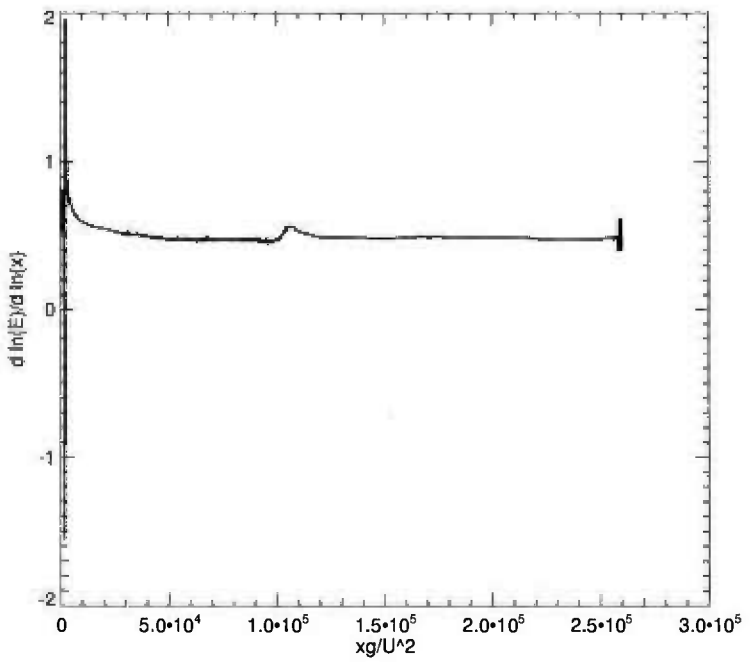

Fig.21 Same as Fig.3, but for Hsiao-Shemdin S_{in}

Dependence of the mean frequency against the fetch shown on Fig.22 demonstrates discrepancy with *ZRP* results and asymptotic value of index $q \approx 0.21$, see Fig. 23

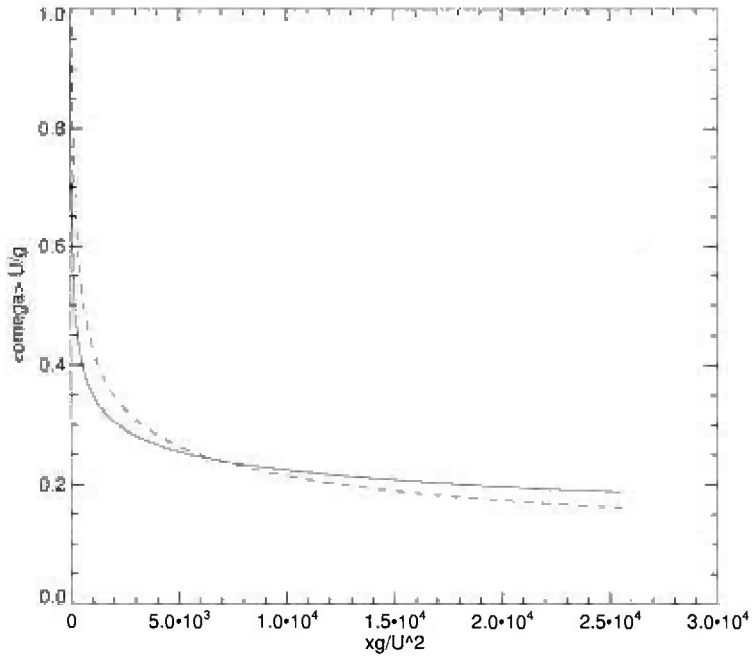

Fig.22 Same as Fig.4, but for Hsiao-Shemdin S_{in}

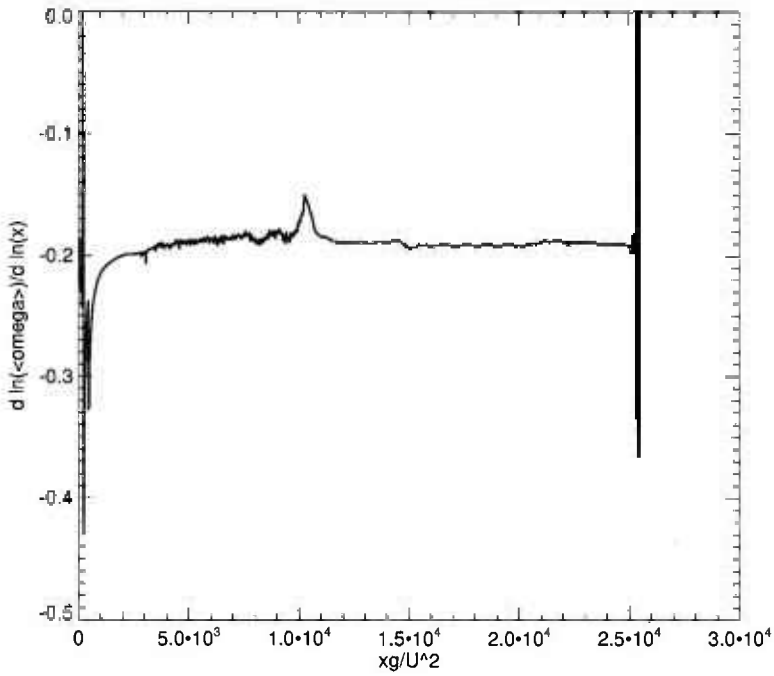

Fig.23 Same as Fig.5, but for Hsiao-Shemdin S_{in}

Fig.24 presents directional spectrum as a function of frequency in logarithmic coordinates. One can see:

1. Spectral maximum area

2. Kolmogorov-Zakharov spectrum ω^{-4}
3. Phillips high frequency tail ω^{-5}

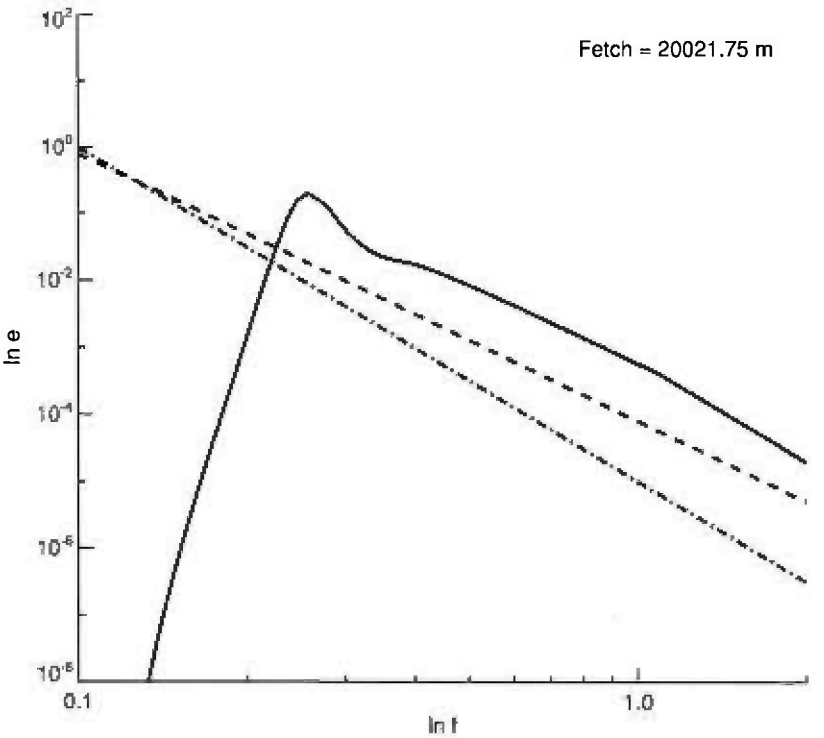

Fig.24 Same as Fig.6, but for Hsiao-Shemdin S_{in}

Fig.25 presents combination ($10q$-$2p$) as the function of the fetch. It is in total agreement with the theoretical predictions Eq.(39), which means that self-similarity is fulfilled locally in Hsiao-Shemdin case.

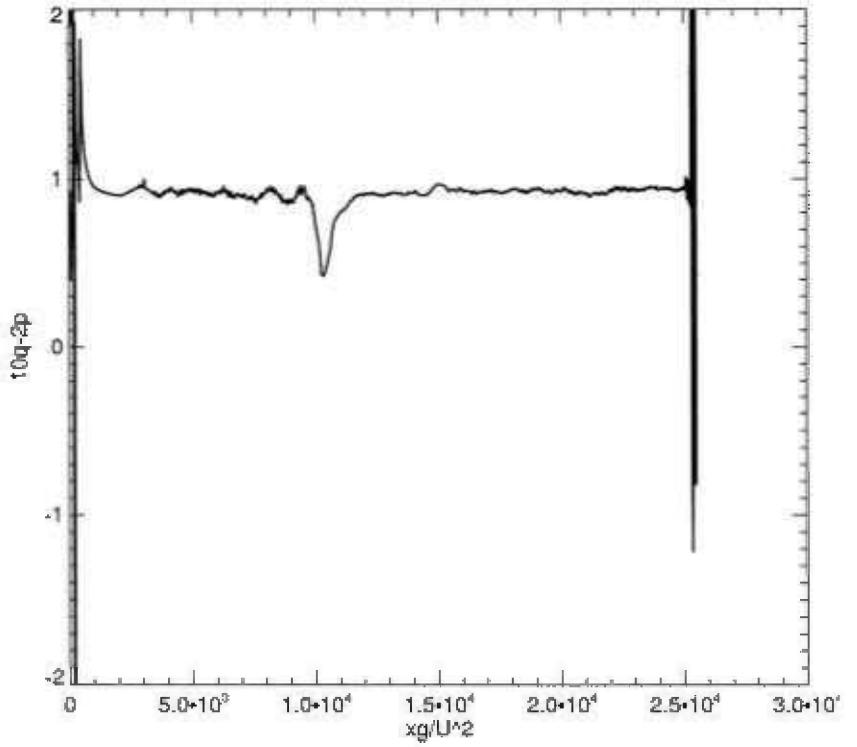

Fig. 25: Relation (10*q*-2*p*) as the function of the fetch for *Hsiao-Shemdin* wind input term.

1.10 Test of WAM3 input terms

WAM cycles 1 through 3 source terms contain not only wind input term, but also long-wave dissipation [R21,R40,R50].

The input source term S_{in} is defined as [R50]

$$S_{in}(k,\theta) = C_{in}\frac{\rho_a}{\rho_w}\max\left[0,\left(\frac{28u_*}{c}\cos(\theta-\theta_0)-1\right)\right]\omega\varepsilon(k,\theta)$$

$$u_* = u_{10}\sqrt{(0.8+0.065u_{10})10^{-3}}$$

where $C_{in} = 0.25$, ρ_a and ρ_w are the densities of air and water, $u_\star$ is the wind friction velocity, c is the wave phase velocity. S_{diss} is defined by Eq. (27)-(29).

Fig.26 shows that total energy growth along the fetch strongly underestimates *ZRP* simulation, and has the value of exponent p asymptotically going to 0 versus the fetch, see Fig.27.

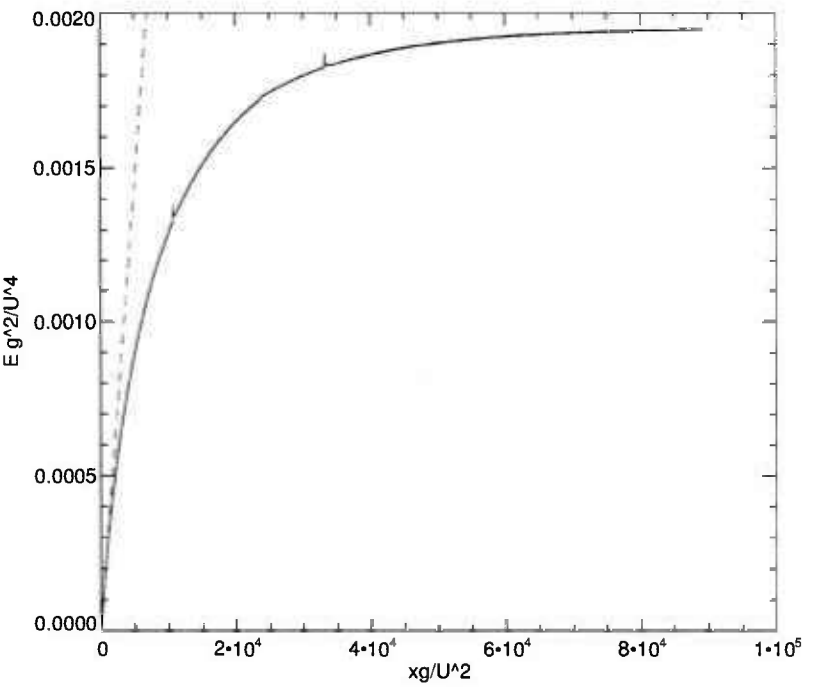

Fig.26 Same as Fig.2 but for *WAM3* S_{in}

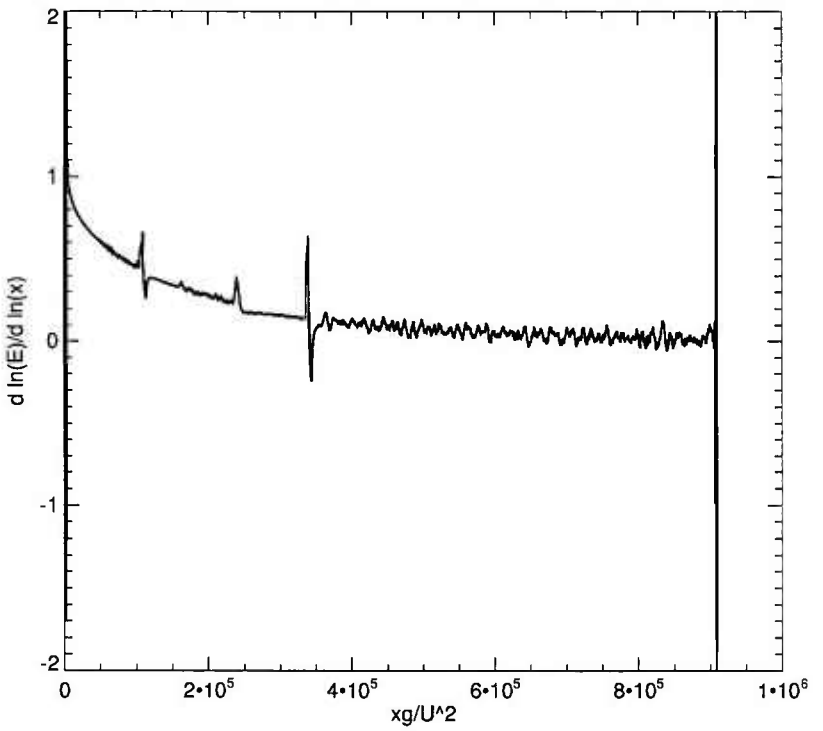

Fig.27 Same as Fig.3, but *WAM3* S_{in}

Dependence of the mean frequency against the fetch shown on Fig.28 demonstrates strong discrepancy with *ZRP* results and the value of the corresponding index q going asymptotically to 0, see Fig.29.

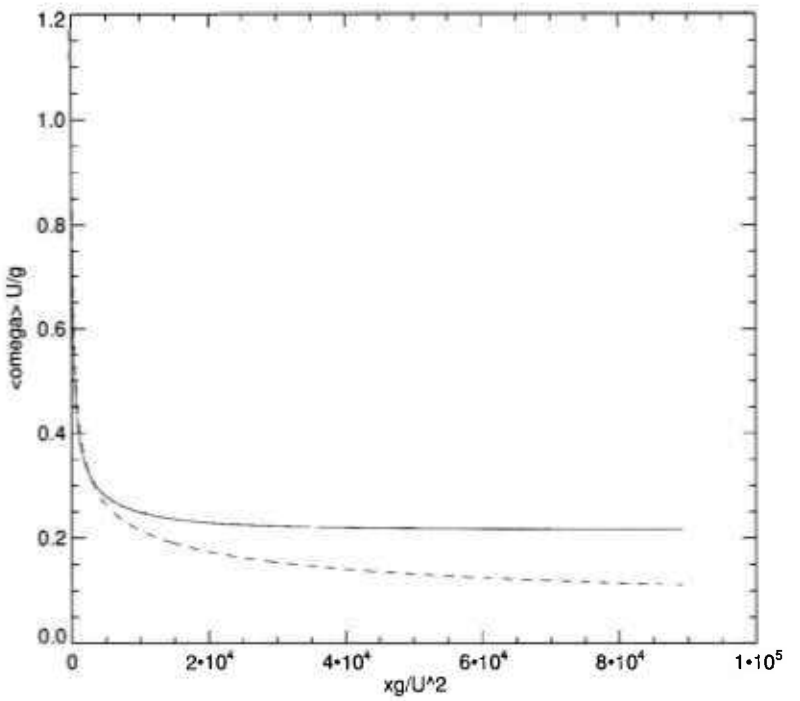

Fig.28 Same as Fig.4, but for *WAM3* S_{in}

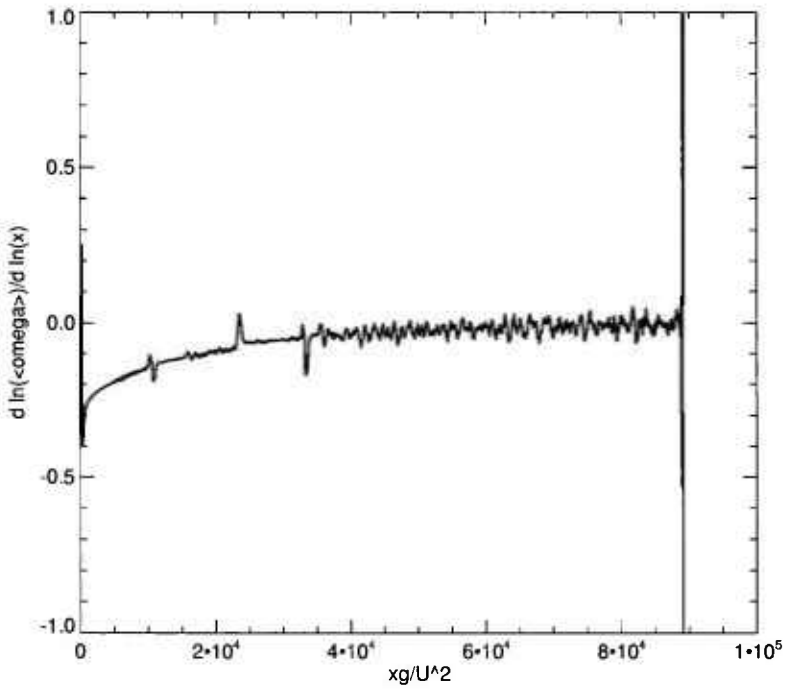

Fig.29 Same as Fig.5, but for *WAM3* S_{in}

Fig.30 presents directional spectrum as a function of frequency in logarithmic coordinates. One can see:

1. Spectral maximum area
2. Kolmogorov-Zakharov spectrum ω^{-4}
3. Phillips high frequency tail ω^{-5}

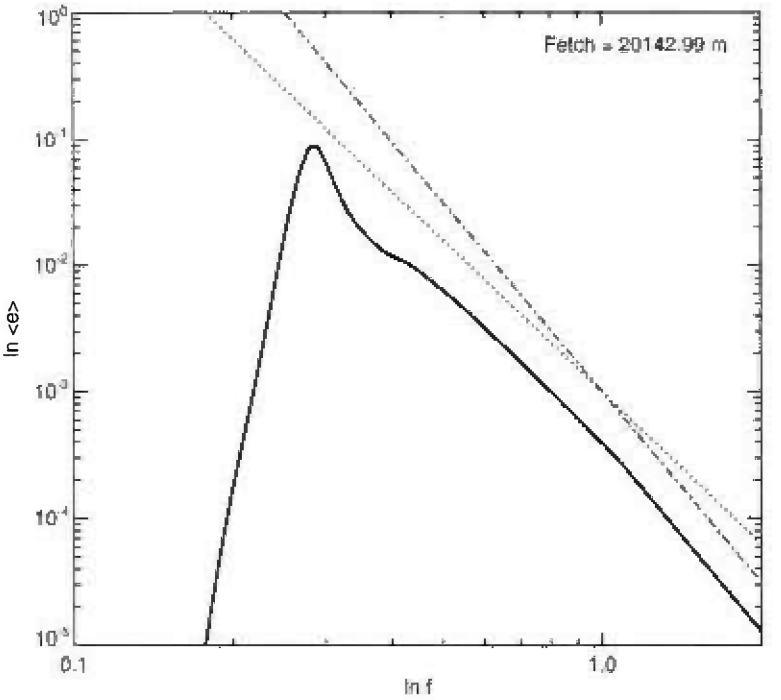

Fig.30 Same as Fig.5, but for *WAM3* S_{in}

Fig. 21 presents combination (10*q*-2*p*) as the function of the fetch. It is in total disagreement with the theoretical predictions. There is no any indication of "magic relation" Eq. (39) fulfillment.

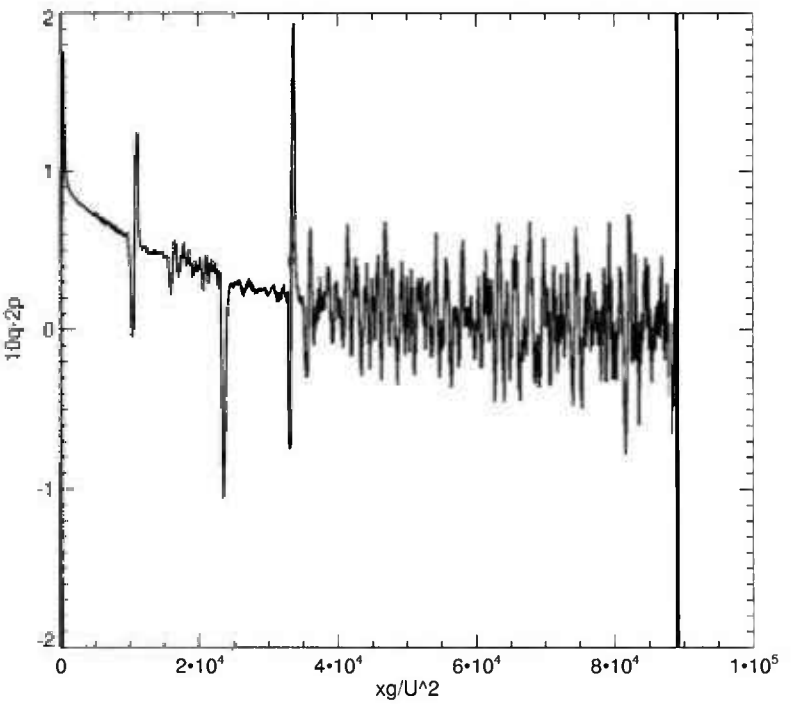

Fig. 31: Combination (10*q*-2*p*) as a function of the fetch for *WAM3* S_{in}

Comparing the results, obtained for Snyder and *WAM*3 wind input terms, we see strong discrepancies. Energy dependence on the fetch for *WAM*3 model (which is essentially Snyder model with long-wave dissipation) strongly qualitatively differs from Snyder model. When long-waves dissipation is present, the energy is not only much smaller, but also its dependence on the fetch stops to be power-one very soon, and radically differs from all other above considered variants of wind forcing lacking long-wave dissipation.

Fig.32 presents plots of angle averaged energy dissipation function and spectral energy. One can see that spectral dissipation in WAM3 model has sharp minimum corresponding to the location of the spectral energy maximum, which confirms the assumption that spectral maximum dissipation plays definitive role in WAM3 model.

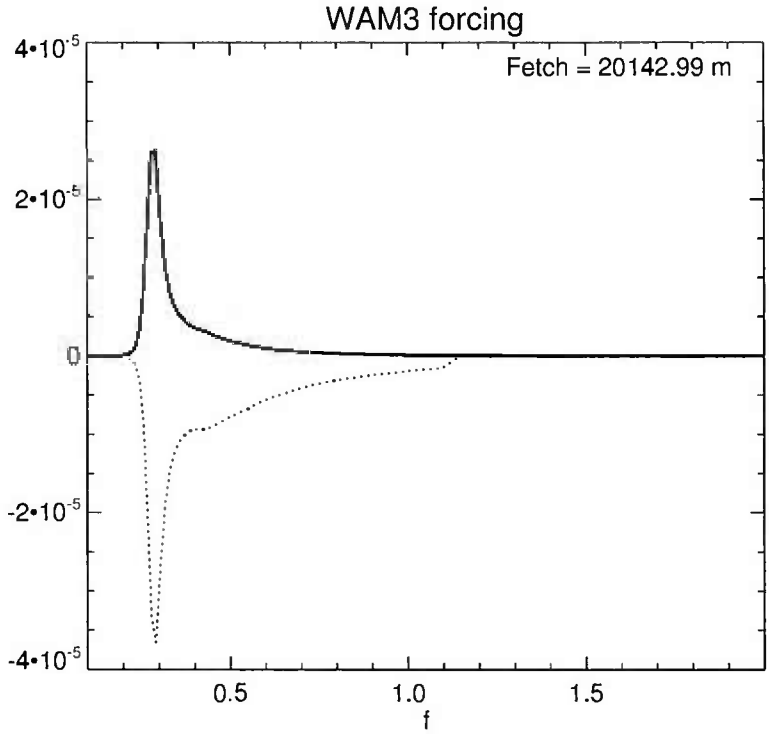

Fig.32 Angular averaged energy dissipation function $\frac{1}{2\pi}\int_0^{2\pi}\gamma_{diss}\varepsilon(\omega,\theta)d\theta$ **(dotted line) and angle averaged scaled energy spectrum** $0.0001\int_0^{2\pi}\varepsilon(\omega,\theta)d\theta$ **(solid line) as the functions of frequency** f**.**

1.11 Summary

We are offering alternative framework for numerical simulation of *HE*. Being supplied with *ZRP* wind input term, such approach reproduces the results of more than a dozen of experimental observations. We also performed numerical simulations of *HE* for four another historically well-known wind input terms within the same alternative framework. They demonstrated the results deviating from *ZRP* simulation.

To classify the results of the above simulations we applied the set of nonlinear tests to different kinds of wind input terms, and here is the conclusion:

1. *ZRP* forcing term perfectly corresponds to theoretically predicted results like Kolmogorov-Zakharov spectrum $\sim \omega^{-4}$, self-similar solutions for energy and frequency with exponents p=1 and q=0.3 correspondingly, "magic relation" $10p$-$2q$=1 and reproduces more than a dozen of field experiments. Therefore, it can serve as the benchmark.
2. All wind input terms pass the test for presence of Kolmogorov-Zakharov law $\varepsilon \sim \omega^{-4}$. This means that effects of nonlinearity are so strong, that presumably no variation of the wind input term parameterization can suppress it.
3. Chalikov and Hsiao-Shemdin cases fail p- and q- tests, but pass "Magic relation" (quasi-self-similarity) test.
4. *Snyder* case "approximately" passes p-, q- and "magic relation" tests. However, numerical value of mean energy exceeds *ZR*P and experimental results by the factor of 5-6 times.
5. *WAM*3 case fails to pass all except *KZ* spectrum test.
6. None of the wind-input parameterization, except *ZRP* one, can correctly reproduce experimentally observed limited fetch growth.

In summary, the nonlinearity influence is so robust in the dynamics of *HE* that one can't "spoil" Kolmogorov-Zakharov law $\sim \omega^{-4}$ for any tested wind input term S_{in}. Self-similarity tests like p- and q-tests are the most sophisticated between suggested ones. And the "magic relation" test is probably somewhere in-between versus detection of the "quality" of particular wind input term.

The analysis of multiple experimental field, laboratory measurements and numerical experiments performed in [**Error! Reference source not found.**] shows universality of "magic relations" fulfillments. That confirms the thesis on nonlinear interactions domination in the wind ocean energy balance.

The summary of the tests is presented in Table 2.

Experiment	p-test	q-test	*KZ*-spectrum	Magic relation	Energy growth
ZRP	YES	YES	YES	YES	YES
Chalikov	NO	NO	YES	YES	NO
Snyder	≈	≈	YES	YES	NO
Hsiao-Shemdin	NO	NO	YES	YES	NO
*WAM*3	NO	NO	YES	NO	NO

Table 2 The summary of the tests

Presented research results are published in [P1], [P2], [P3] and [P4].

2. Basic features of kinetic Hasselmann equation for wind-driven seas and their applications

This section is devoted to studies of basic features of the kinetic Hasselmann equation that determine the leading role of the nonlinear transfer. It provides an opportunity for developing an asymptotic approach and, then, deriving a series of quite concise relationships for parameters of growing seas and swell. We start with a demonstration of the leading role of nonlinear transfer and propose asymptotic estimates of relaxation scales of the spectra of wind-driven waves [R7,R20]. It gives a ground for use an asymptotic approach for wind-driven seas in a spirit of our previous works [R16,R17]. Then we use simple relationships for analysis of Voluntary Observing Ships data [R70]. One more experimental application of the asymptotic theory is presented as a physical model for retrieving wave periods from satellite altimetry data [R71]. The concept of the generalized Phillips' spectra is presented as a synthesis of the asymptotic theory and a heuristic theory of wave dissipation that leads to the classic Phillips spectrum $E \sim \omega^{-5}$ [R56]. The series of the work on the asymptotic methods for the kinetic equation for wind waves is finalized by very important and surprising result: we present a universal invariant that links steepness and wave field lifetime expressed in terms of dimensionless wave periods or wavelengths [R19]. The latter work opens fair prospects both as a tool of verification of wave forecasting models and for developing new experimental approaches.

2.1 Energy balance in wind-driven seas within the Hasselmann equation

The problem of balance of different terms in the right-hand side of the Hasselmann equation (1) is a key question for both wind-wave interaction theory and modeling. Today's mainstream emphasis is on developing new functions S_{in} and S_{diss}, but not correct and accurate calculation S_{nl}. Confusion comes from [R21], where all three source terms have been compared for the case of fully-developed (mature) sea, and conclusion has been made that terms S_{in} and S_{diss} can be two-three times greater than S_{nl}. We show, in fact, that situation is opposite: S_{nl} has a leading role in balance of wind-driven seas. The analysis is based on decomposition of S_{nl} into nonlinear damping $\Gamma_k N_k$ and forcing F_k

$$S_{nl} = F_k - \Gamma_k N_k \qquad (47)$$

where Γ_k – positive nonlinear damping decrement, N_k – spectral density of wave action. Our numerical and analytical results show that $\Gamma_k N_k$ and F_k surpass conventional parameterizations of input and dissipation of wind-driven waves by, at least, one order of magnitude, see Fig.33.

An additional argumentation is presented in Fig.2, where nonlinear damping decrement $\Gamma_k N_k$ is compared to empirical parameterizations of wind-wave growth given by different authors and used in the today wave forecasting models as an option [R72-R40].

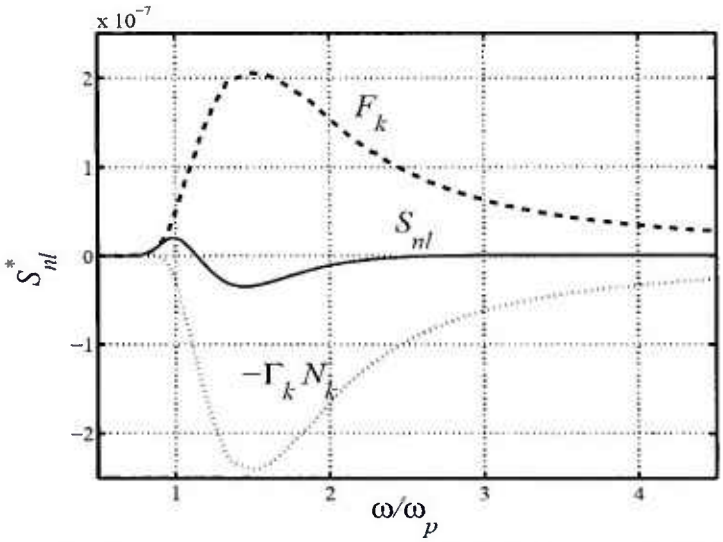

Fig.33 Decomposition of the nonlinear term S_{nl} (solid line) for the case by Komen et al. (1984) [R71] into nonlinear forcing (dashed) and damping (dotted) terms (see Eq.47)

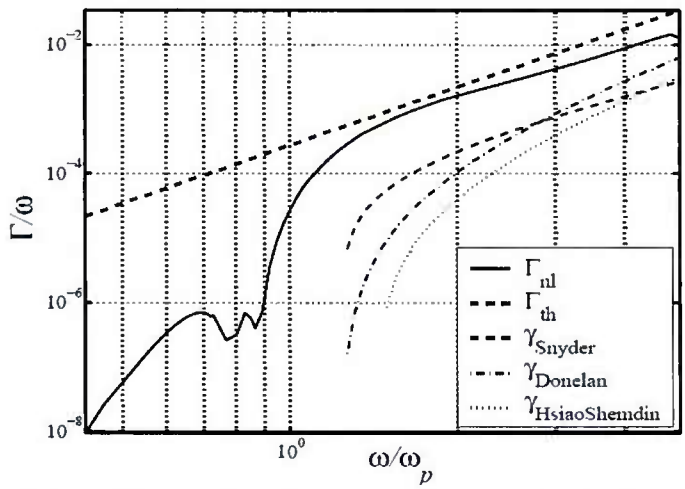

Fig.34 Nonlinear damping coefficient Γ_k given by theoretical estimate and by the numerical simulation (dashed and solid bold curves, correspondingly). Conventional dependencies of wind growth increments are shown by thin curves with authors' names in the legend

Our result on dominating effect of nonlinear interaction on wave spectra evolution should not be interpreted as a call to ignore the effects of wind input and wave dissipation. The leadership of S_{nl} does not mean that we disregard wind input and dissipation, we just put them in proper place. The strong nonlinear forcing and damping that compose the conservative term S_{nl} determine strong relaxation and a universality of spectral shaping due to inherent wave dynamics, while S_{in} and S_{diss} are responsible for growth of total energy.

Obtained result will help to make better theoretical estimates of solutions of Hasselmann equation and help to develop simplified approximations to source terms. An important direction of the result application is the use of asymptotic relationships for analysis of experimental data.

2.2 Global visual observations as a tool for discriminating swell and wind seas

Simple asymptotic relationships of the asymptotic theory for the case of dominating nonlinear transfer can be used for analysis of experimental data. In this part of the project we use the most abandoned source of data the Voluntary Observing Ships (VOS) data. Generally, these data are considered as a source of information on climatic features of the world ocean rather than experimental background of studies of physical mechanisms of wind-wave dynamics. We are trying to change this tradition by applying results of asymptotic weakly turbulent model of wind-driven seas [R20,R3] to extensive data base of the Global Atlas of Ocean Waves [R73-R74].

The global visual wave observations are re-analyzed within the theoretical concept of self-similar wind-driven seas. The theoretical criteria of discriminating wind-driven and swell seas are formulated and shown to be adequate to the problem. The results are detailed for the South Pacifica, which wave climatology based on VOS data is well studied and the swell component is well pronounced. The core of the analysis are one-parametric dependencies "wave height - wave period" $H_s = CT^Z$. The reference cases [R75-R76] have found, correspondingly, $Z = 5/3$, $Z = 3/2$ and $Z = 4/3$. This set of exponents Z has been interpreted recently in [R17,R18] in terms of spectral fluxes and total wave input. An alternative reference case – sea swell gives an opposite signature of the exponent $Z = -1/2$. This simple criterion was used and appeared to be robust for the problem of swell-wind sea discrimination.

The corresponding exponent Z appears to be slightly higher than $Z = -1/2$, that implies a pumping of sea swell by wind-driven sea background [R70]. This important issue is considered both in the context of methodology of obtaining VOS data and within the physics of the mixed sea. This result contradicts to commonly accepted vision of sea swell as a neutral or slightly decaying fraction of ocean wave field.

Prospects of further study are quite promising. In particular, satellite data are seen to be used for tracking ocean swell and for studies of physical mechanisms of its evolution.

Fig.35 gives a graphical summary of four reference cases of self-similar evolution of wind-driven waves. These cases are shown as different R, tangents of one-parametric dependencies

$$H \sim T^R$$

height-to-period in logarithmic axes. Reference cases of growing wind sea are shown as the young sea growth at permanent wave momentum production (exponent $R = 5/3$ by Hasselmann et al. 1976 [R75]), growing Toba's sea ($R = 3/2$) and old premature sea by Zakharov and Zaslavsky 1983 [R76] with $R = 4/3$.

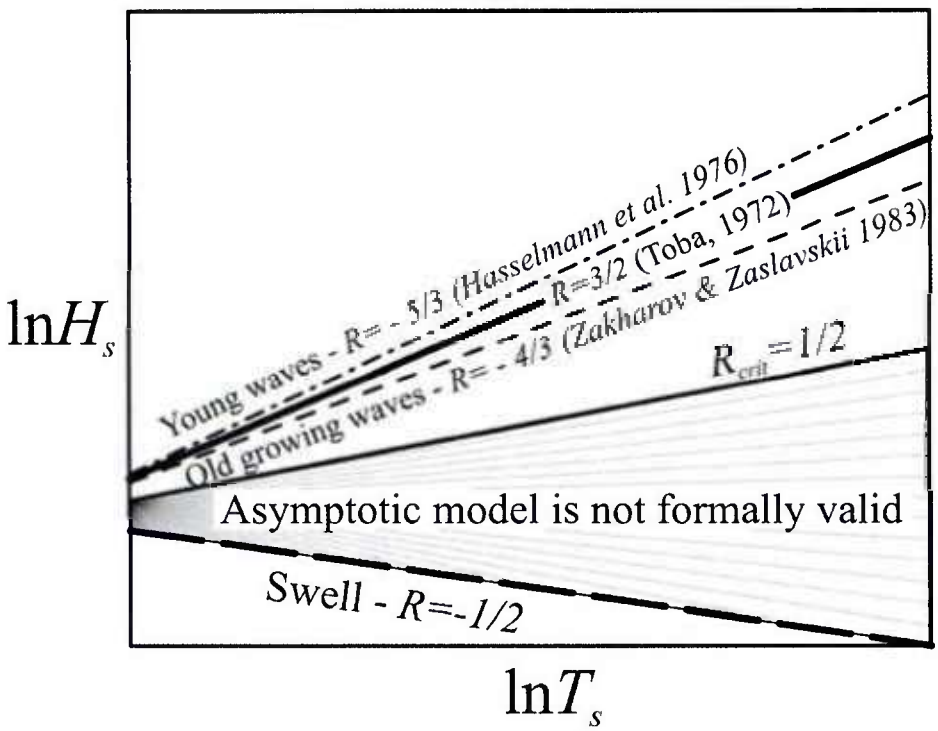

Fig. 35 Reference cases of wave growth as one-parametric dependencies $H_s(T_s)$. Cases of Toba [1972] R = 3/2 law and swell with R = -1/2 are shown by bold lines. Domain where the asymptotic scheme is formally invalid (Badulin et al., 2007 [R74]) is shaded.

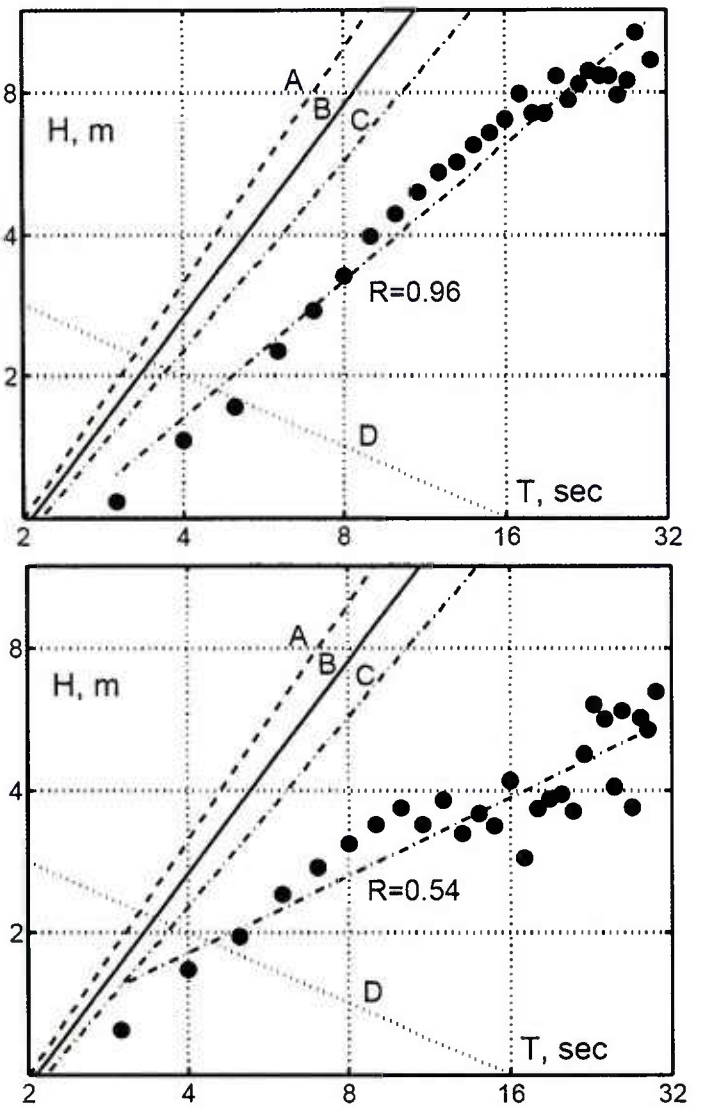

Fig.36 Dependencies H(T) and their power law fits for the whole World Ocean, 1970–2007 for (top) wind waves and (bottom) swell. Lines marked as A, B, C, D show reference power laws of Fig.5. The exponents of the experimental fits R = 0.96 for wind sea and R = 0.54 for swell are found to be quite far from the reference cases. Totally, 36,356,695 reports have been used for wind waves and 31,041,169 for swell observations.

The height-to-period dependencies *H(T)* derived from the VOS data are shown in Fig.36 for visually delineated wind waves (upper panel) and swell (bottom panel). The difference of these two cases is clearly seen in terms of exponents *R*. Thorough analysis of the experimental data uncovers more physically significant difference of two sea waves extremes. Selecting waves in wave ages and, what is more important, in wave periods we found definite indications on pumping of swell. Results of such selection are illustrated by Fig.37 where histograms of exponents *R* estimated for 20° by 20° coordinate boxes are given. While for the wind waves the histogram is localized near a value more than 1, for swell the corresponding distribution is quite large that implies a variety of physical mechanisms responsible for the swell dynamics.

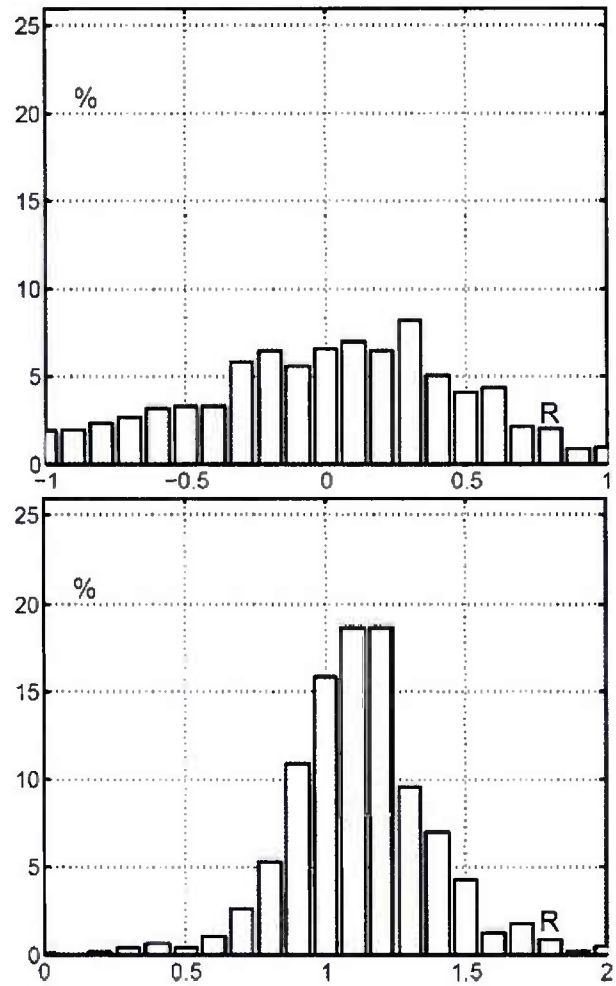

Fig. 37 Histograms of exponents R of power law fits of H(T) dependencies calculated monthly for 20x 20 boxes of the World Ocean (1481 dependencies of total 1782 = 8 x18x12 coordinate boxes) for special ranges of wave periods: (bottom) wind sea with T = 5–10 s and (top) swell with periods T = 10–20 s.

With the exponent *R* as indicator of sea wave dynamics we make a conceptual step: we study a link of wave heights *H* and periods *T* rather than features of the independent data sets. The separate analysis basing on VOS (Gulev et al., 2004 [R73]) or satellite data (e.g., Zieger, 2010 [21]) gives valuable information on ranges of wave parameters and their geographical variability, but propose quite primitive vision of wave dynamics. Recent attempts to combine satellite altimeter observations of wave heights and mathematical modeling of wave dynamics (Laugel et al., 2012 [R77]) propose reconstructions of full spatio-temporal structure of wind wave field. This study is based on extensive simulations and requires thorough theoretical analysis. The interpretation of its results in the context of burning problems of sea wave physics shows a good prospect for further study.

2.3 Physical model of sea wave period from altimeter data

Satellite measurements are the next very prospective source of sea wave data. Data of satellite altimetry are the most abundant source of data. Accuracy of measurements of wave height by satellite altimeter is higher than the majority of in situ methods. At the same time these devices cannot measure wave periods. The latter important characteristics of wave field are generally estimated indirectly, as a rule, from empirical dependencies of the measured wave height and radar cross-section.

We use the asymptotic theory of wind wave growth proposed in [R17] that predicts the Kolmogorov - like relationship between instant total wave energy $\boldsymbol{E}$ and total net wave forcing $\boldsymbol{S}$ (wave input minus dissipation). The latter can be associated with the observed rate of wave energy $\boldsymbol{dE/dt}$. Inversion of the so-called weakly turbulent law of wind-wave growth (see Eq. (1.9) in [R17]) gives a simple formula for period of spectral peak $\boldsymbol{T_p}$ as a function of significant wave height $\boldsymbol{H_s}$ and its gradient. The relationship can be used for processing altimeter data assuming the wave field to be stationary and spatially inhomogeneous. It is consistent with satellite measurements setup and is written as follows

$$T_p=2^{1/5}\alpha_{ss}^{-3/10}(H_s/g)^{1/2}\times(\partial H_s/\partial s)^{-1/10} \qquad (48)$$

Self-similarity parameter in Eq.(48) is set constant α_{ss}=0.67.67 as found in recent simulations of wind wave growth [R18]. Wave height derivative along the wave propagation (group velocity) $\partial H_s/\partial s$ enters Eq.(48) in very low power *1/10* that reduces dramatically the effect of the unknown wave direction relative to the satellite track where the derivative can be estimated.

In contrast to all the models of wave periods mentioned above, Eq.(48) does not contain any empirical coefficients and, thus, does not require calibration. Additionally, it does not operate with backscatter coefficient σ_0,, which characterizes sea surface roughness in gravity-capillary range and cannot be related to dominant waves straightforwardly.

The proposed method relies upon weakly turbulent mechanisms when instant sea state is determined by external flux to/from waves. The instant state and its apparent perturbation rate recorded by spatial derivative $\partial H_s/\partial s$ allow one to estimate wave period in certain range of scales. These scales should be sufficiently long as compared to the relaxation scales of weakly nonlinear surface waves and relatively short as compared to typical scales of variability of the wave field. Typical distance between two consecutive counts of satellite altimeter 5-7 kilometers (1 second) likely satisfies these simple criteria for sea waves and allows Eq.(48) to capture the weakly turbulent mechanism of wind-wave growth.

The new algorithm has been tested for the data collection of the ESA initiative Globwave (*http://www.globwave.org*). Different empirical models have been compared both for along-track records and in terms of statistical distributions of wave characteristics for particular ocean regions.

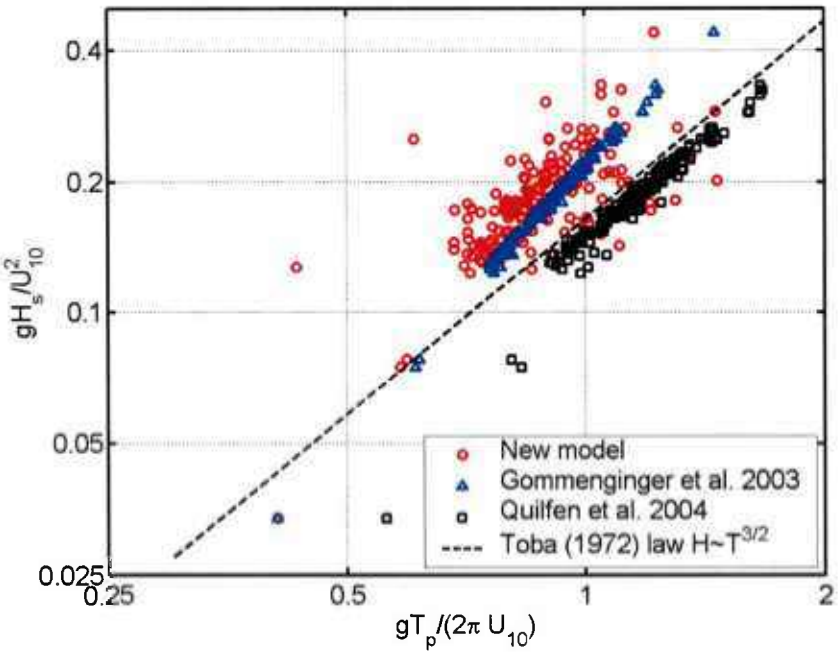

Fig. 38 Dependencies of non-dimensional wave height on non-dimensional wave period (wave age) calculated by different methods (see legend) for 800 km track of JASON-2 in the Caspian Sea, June 2, 2012.

Fig.38 presents an example of along-track evolution of non-dimensional wave height and period (wave age) calculated within different approaches [R78-R79]. The new model shows good agreement with previously proposed empirical dependencies. Relatively high dispersion of the new method (red points) can be partially explained by intentionally coarse data processing when neither smoothing nor interpolation of data has been used. At the same time, strong collapsing of results of calculations with [R78-R79] in Fig.38 looks suspicious enough: in situ experiments do show rather high dispersion relatively to "reference" growth curves like one of [R69]. As our study shows, the "impoverishing" wave dynamics within the empirical parameterizations of wave period is well pronounced both for along-track cases like one presented above and in terms of statistical distributions for subsets of the Globwave data collection.

This study presents the very first results of the new model for wave periods from satellite altimeter data. The model is free of any empirical and tuning parameters, therefore, is independent on features of particular altimeter devices (if properly calibrated in wave height Hs) and regional peculiarities (say, extreme salinity in some inland basins).

Agreement with previously proposed approaches points to the validity of the asymptotic weakly turbulent law the new method is based on. While having very few in situ evidences of validity of the weakly turbulence theory for the wind-driven sea for the last 50 years, one has billions satellite altimeter records that are consistent with conclusions of this theory.

2.4 Universality of wind-wave growth

For developing the physical model for satellite altimetry measurements we used the form of the so-called weakly turbulent law [R17]. A remarkable fact is that similar law can be rewritten in a

remarkably concise form of invariant that links instant wave steepness and time or fetch of wave development expressed in wave periods or lengths

$$\mu^4 \nu = \alpha_0^3 \tag{49}$$

Here $\mu = {E^{1/2}\omega_p^2}/{g}$ is wave steepness defined in terms of total wave energy E and spectral peak frequency ω_p, ν is a number of waves. For the duration-limited setup one has

$$\nu = \omega_p t \tag{50}$$

For the fetch-limited case we keep

$$\nu = 2k_p x \tag{51}$$

where coefficient 2 reflects the ratio of phase and group velocity of deep water waves. The universal constant α_0 in Eq. (49) has to take different values for duration- and fetch-limited setups. We introduce two different constants $\alpha_{0(d)} = 0.7$ and $\alpha_{0(f)} = 0.62$ based on our previous numerical and experimental studies [R17,R80].

The law Eq. (49) does not contain wind-sea interaction parameters explicitly and relies upon asymptotic theory where wave nonlinearity is assumed to be a leading physical mechanism. The validity of this law is illustrated by results of numerical simulations of growing wind seas.

Fig.39 shows the results of simulations of duration-limited growth within the Hasselmann equation with the exact calculation of nonlinear term. The strong tendency of the invariant Eq. (49) to attract the theoretical limit $\alpha_{0\{d\}} = 0.7$ is seen fairly well.

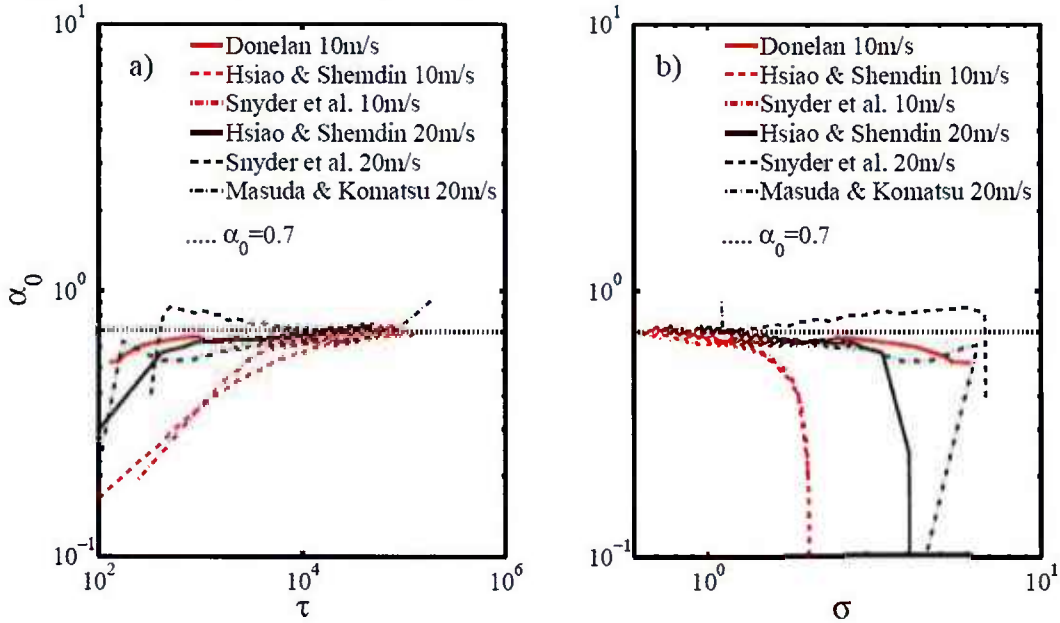

Fig.39 Dependence of parameter $\alpha_0 = (\mu^4 \nu)^{1/3}$: (a) non-dimensional duration $\tau = gt/U_{10}$ and (b) inverse wave age $\sigma = \omega_p U_{10}/g$ in simulations of duration-limited wind wave growth [R20,R17,R80]. Simulation setups (wind input parameterization and wind speed) are given in legends. The horizontal dotted line shows theoretical value $\alpha_{0(d)} = 0.7$.

The case of fetch-limited setup has been considered in terms of dimensionless dependencies of wave height on wave period. Within the proposed approach that does not rely upon wind parameters and dimensionless variables can be introduced as follows for duration-

$$\tilde{H} = H/gt^2; \quad \tilde{T} = T/2\pi t \tag{52}$$

and fetch-limited setups

$$\tilde{H} = H/x; \quad \tilde{T} = T\sqrt{g/8\pi^2 x} \tag{53}$$

Simulations of the fetch-limited growth have been carried out by A. Pushkarev (Pushkarev, Zakharov, 2012) and used considered evolution of wave spectra both in time and space. Fig.40 shows an intermediate nature of asymptotic of the solutions. In the left panel the scaling Eq.(53) has been used. The fetch-limited asymptotical dependence

$$\tilde{H} = 5.59\tilde{T}^{5/2}$$

works quite well in a range. For large time the corresponding curves are tending to a saturation: wave field start to develop in a duration-limited regime.

The right panel of Fig.40 shows the same results in terms of time scaling Eq. (52) that gives the law

$$\tilde{H} = 3.06\tilde{T}^{9/4}$$

Again, we see proximity of the simulation results to the theoretical curve in an intermediate range of dimensionless wave periods.

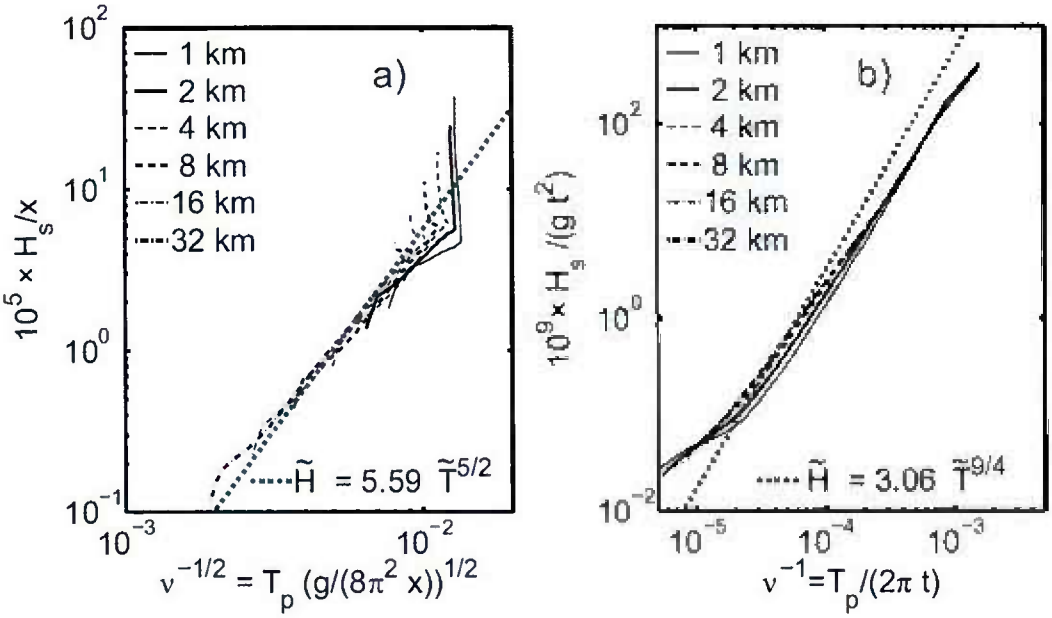

Fig.40 Wave growth curves in simulations of fetch-limited setup (Pushkarev, Zakharov, 2012) within: (a) fetch scaling; (b) duration scaling. Curves are given for fixed fetches 1, 2, 4, 8, 16, 32 km (see legends). Theoretical dependencies are shown by dotted lines.

Thus, the proposed theoretical law Eq.(49) is verified in an extensive numerical study and provides the tool for diagnosis of wind wave growth.

2.5 Summary

We see that our asymptotic approach based on assumption of the dominating nonlinearity in the Hasselmann equation gives important results both for the wave theory and numerous applications including experimental approaches for satellite studies from space.

The results have been published in [P5]-[P12].

3. Dynamical equations for surface waves and their applications

New compact equations describing water waves moving in one horizontal direction were derived. This equation (compact Dyachenko - Zakharov equation) was generalized for "almost" 1D waves, in other words waves slightly modulated in the transverse direction.

Using this equation we have performed the set of the following numerical experiments:

1. Simulation of nonlinear stage of modulational instability of wave train.
2. Simulation of breathers collisions (localized solutions of the equation).
3. Simulation of freak-waves appearing in 1-D and 2-D situations
4. Simulation of freak-waves in the frame of new compact equations, which showed the same results as fully nonlinear equations for water waves.
5. Simulation of relaxation of JONSWAP spectrum for water waves

Also, it was proven analytically non-integrability of the equation and exact breather type solution was found (like soliton for NLSE).

3.1 New canonical equation for one-dimensional surface waves

We applied canonical transformation to the water wave Hamiltonian

$$H=\frac{1}{2}\int(\psi\hat{k}\psi+g\eta^2)dx+\frac{1}{2}\int\eta\{\psi_x^2-(\hat{k}\psi)^2\}dx+\frac{1}{2}\int\eta(\hat{k}\psi)\{\hat{k}(\eta(\hat{k}\psi))+\eta\psi_{xx}\}dx$$

where

$$\psi(x,t)=\phi(x,y,t)\big|_{y=\eta}=\phi(x,\eta(x,t),t).$$

The transformation removes not only cubic nonlinear terms, but simplifies drastically fourth order terms in the Hamiltonian:

$$H=\int b^*\hat{\omega}_k b dx+\frac{1}{4}\int|b'|^2\left[\frac{i}{2}(bb'^*-b^*b')-\hat{k}\,|b|^2\right]dx.$$

b – is new normal canonical variable. This transformation explicitly uses the fact of vanishing exact four waves interaction for water gravity waves for 2D potential fluid. After the transformation well-known but cumbersome Zakharov equation is drastically simplified and can be written in X-space in compact way. This new equation is very suitable for both analytic study and numerical simulation:

$$i\frac{\partial b}{\partial t}=\hat{\omega}_k b+\frac{i}{8}\left[b^*\frac{\partial}{\partial x}(b'^2)-\frac{\partial}{\partial x}(b^{*\prime}\frac{\partial}{\partial x}b^2)\right]-\frac{1}{4}\left[b\cdot\hat{k}(|b'|^2)-\frac{\partial}{\partial x}(b'\hat{k}(|b|^2))\right].$$

Also, this equation is convenient for experimentalists. The simplest solution of the equation is the monochromatic wave $b(x)=B_0e^{i(k_0x-\omega_0t)}$ with the frequency $\omega_0=\omega_{k_0}+\frac{1}{2}k_0^3|B_0|^2$. Growth-rate of modulation instability is also calculated:

$$\gamma_k^2=\frac{1}{8}\frac{\omega_{k_0}^2}{k_0^4}(1-6\mu^2)k^2\left[\mu^2(k_0-\frac{|k|}{2})^2-\frac{k^2}{8}\right].$$

In the framework of this "improved" Zakharov equation we have performed numerical simulation of freak-wave formation from the initially uniform water waves, see Fig.41

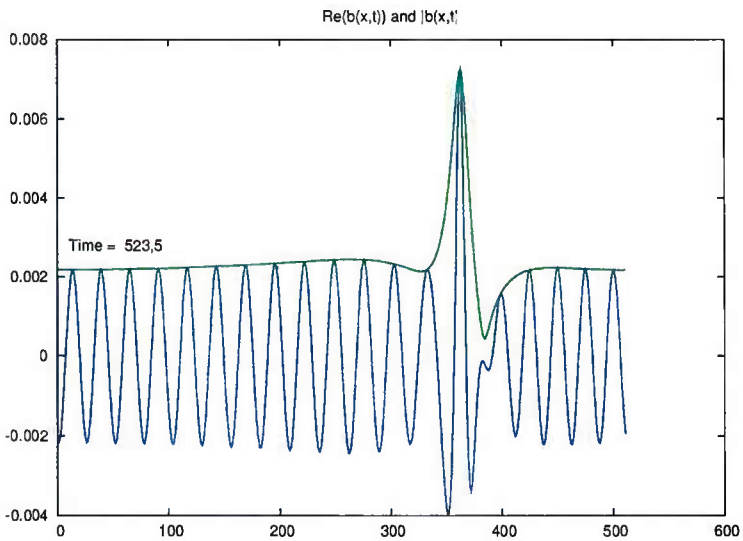

Fig.41 $|b(x)|$ **and** $Re(b(x))$.

We developed simple new equation for 1D nonlinear surface waves, which is convenient for both theoretical study and numerical simulation of wave propagation in narrow experimental tanks.

3.2 Analytical and numerical proof of non-integrability of 2D free-surface hydrodynamics

We studied the problem of integrabily of 2D hydrodynamics of fluid with free surface in a gravity field. This conjecture was formulated in 1994. Here we studied the integrability for potential motion in the framework of Hamiltonian truncated equation up to the fourth order:

$$H = \frac{1}{2}\int g\eta^2 + \psi\hat{k}\psi dx - \frac{1}{2}\int\{(\hat{k}\psi)^2 - (\psi_x)^2\}\eta dx + \frac{1}{2}\int\{\psi_{xx}\eta^2\hat{k}\psi + \psi\hat{k}(\eta\hat{k}(\eta\hat{k}\psi))\}dx + \ldots \quad (54)$$

here $\eta(x,t)$ is the shape of a surface, $\psi(x,t)$ is a potential function of the flow given at the surface and g is gravitational acceleration. To simplify the Hamiltonian we applied canonical transformation which excludes all non-resonant terms and instead of (54) we deal with the equivalent Hamiltonian

$$H = \int b^*\hat{\omega}_k b dx + \frac{1}{2}\int\left|\frac{\partial b}{\partial x}\right|^2\left[\frac{i}{2}\left(b\frac{\partial b^*}{\partial x} - b^*\frac{\partial b}{\partial x}\right) - \hat{K}\,|\,b\,|^2\right]dx.$$

here $\hat{k}$ is the operator multiplying Fourier harmonics by modulus of wave numbers. Corresponding equation of motion is:

$$i\frac{\partial b}{\hat{c}t} = \hat{\omega}_k b + \frac{i}{4}\hat{P}^+\left[b^*\frac{\partial}{\partial x}(b'^2) - \frac{\partial}{\partial x}(b^{*\prime}\frac{\partial}{\partial x}b^2)\right] - \frac{1}{2}\hat{P}^+\left[b\cdot\hat{K}(|\,b'\,|^2) - \frac{\partial}{\partial x}(b'\hat{K}(|\,b\,|^2))\right],$$

This equation has localized breather-type solution

$$b(x,t) = B(x - Vt)e^{i(k_0 x - \omega_0 t)},$$

where k_0 is the wavenumber of the carrier wave, V is the group velocity and ω_0 is the frequency close to ω_{k_0}. In the Fourier space breather can be written as follow:

$$b_k(t) = e^{-i(\Omega t + Vk)}\phi_k,$$

where Ω is close to $\omega_{k_0}/2$. This solution is stable and does not radiate. In the integrable systems collisions of such beaters must be elastic. We performed numerical simulation of collisions of two breathers and have found that it is not pure elastic, see Fig.42.

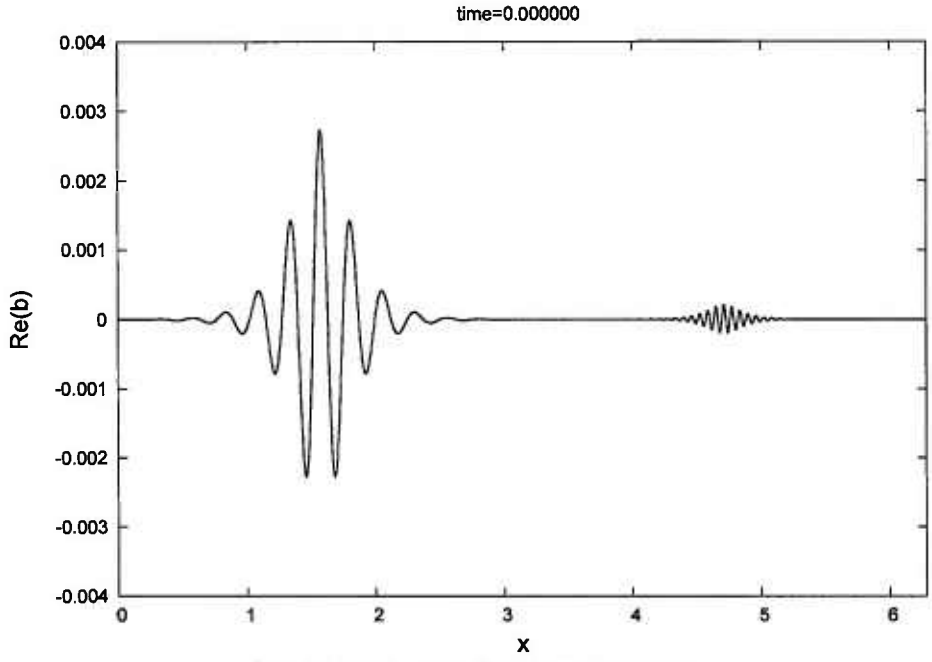

Fig.42 Surface profile of two breathers.

Also we studied analytically coefficient of 6-waves interaction as a superposition of 4-waves interaction. For integrable system it must be equal to zero on the resonance manifold. However, it was found that it does not vanish. So, both numerical and analytical study allows us to conclude that 2-D free surface hydrodynamics is not integrable system.

3.3 Proof of non-integrability of 1-D Zakharov equation and generalization of compact equation for almost 1-D waves

We studied amplitudes of six-wave interactions for compact 1-D Zakharov equation, Hamiltonian of which is:

$$H = \int b^* \hat{\omega}_k b dx + \frac{1}{2}\int |b'|^2 \left[\frac{i}{2}(bb'^* - b^* b') - \hat{k}|b|^2\right] dx.$$

where $b' = \frac{\partial b}{\partial x}$, $\omega_k = \sqrt{gk}$ and $\hat{k}$ - modulus k operator.

It was found that six-wave amplitude (consisted of two four-wave amplitudes) is not canceled for this equation on the resonant manifold. Thus, it was proven that 1-D Zakharov equation is not integrable.

Also we have presented the results of numerical experiments on long time evolution and collisions of breathers (which correspond to envelope solitons in the NLSE approximation) at the surface of deep ideal fluid. The collisions happen to be non-elastic. In the numerical experiment "non-elasticity" can be observed only after many acts of interactions (collisions). This supports "deep water non-integrability" numerically. One can see small radiation after 100 collisions of two breathers (solitons) on Fig. 43:

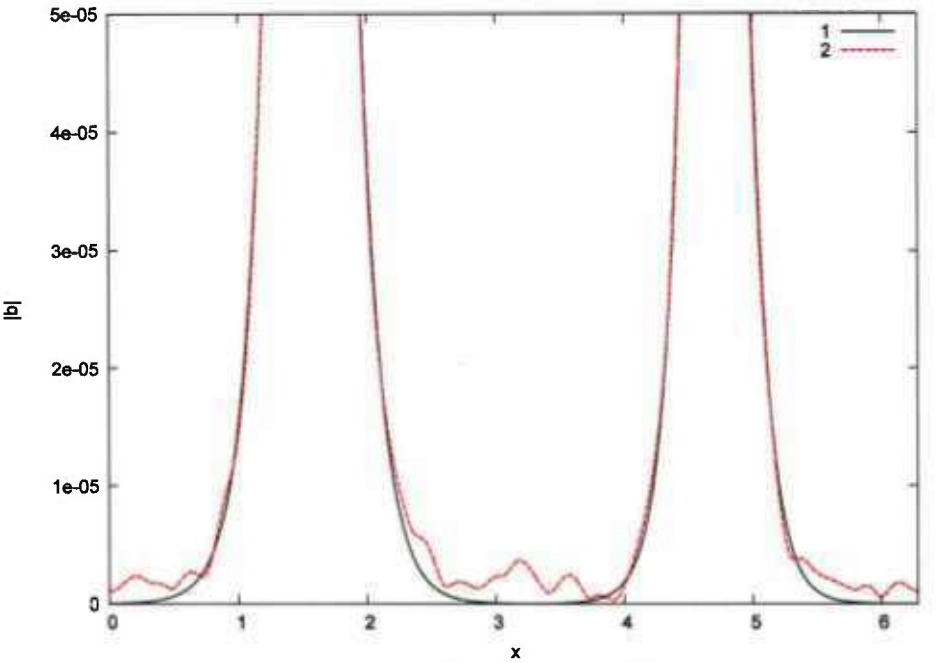

Fig.43 Appearance of small radiation (red line) as a result of 100 collisions of two breathers (black line)

We have derived generalization of compact equation for almost 1-D water waves, slightly modulated in transverse direction with the Hamiltonian as following:

$$H = \int b^* \hat{\omega}_{k_x,k_y} b dx dy + \frac{1}{2}\int |\, b'_x\,|^2 \left[\frac{i}{2}(b b'^*_x - b^* b'_x) - \hat{K}_x\,|\, b\,|^2\right] dx dy.$$

Preliminary numerical experiments on freak-wave formation at the surface of 3D fluids were performed in the framework of this model. Typical picture of the surface with a freak wave is shown below on Fig.44 :

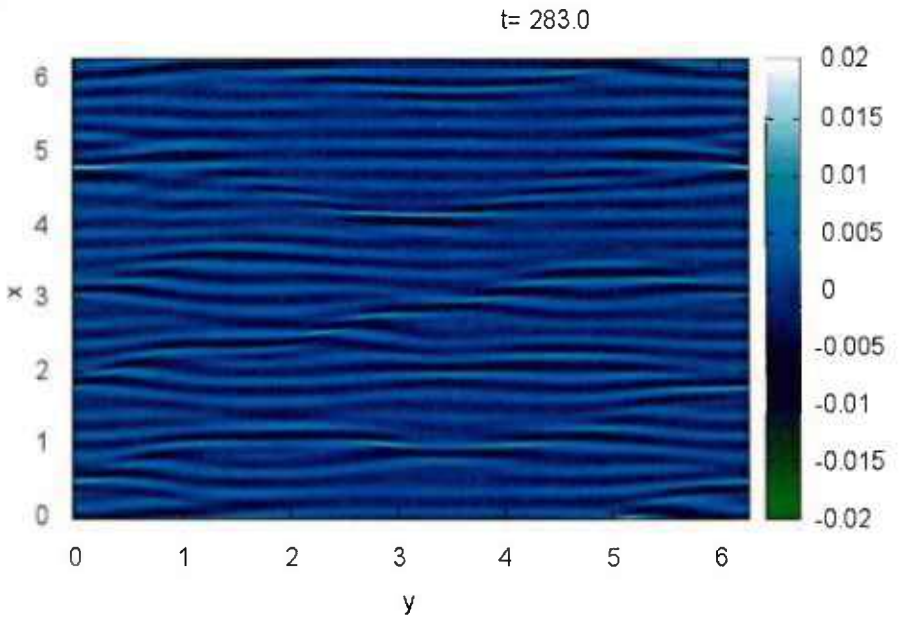

Fig.44 Typical picture of the surface with a freak waves as a result of numerical simulation of generalization of compact equation for almost 1-D water waves

3.4 Comparison of compact equation for surface waves with fully nonlinear equations

We compare applicability of the recently derived compact equation for surface waves with the fully nonlinear equations. Strongly nonlinear phenomena, namely modulational instability and breathers with the steepness $\mu \approx 0.4$ are compared in numerical simulations using both models.

For the fully nonlinear model we have chosen free surface equation written in the conformal variables, $R-V$ -equations [R81] :

$$R_t = i(UR_w - RU_w), V_t = i(UV_w - RB_w) + g(R-1) \tag{55}$$

Now U and B are the following:

$$U = \hat{P}(V\overline{R} + \overline{V}R) B = \hat{P}(V\overline{V})$$

So, these exact Eq. (55) gives us reference solutions to compare with.

For the approximate model we used compact equations derived in [P37], [P38] :

$$\begin{aligned} & i\frac{\partial b}{\partial t} = \hat{\omega}_k b + \frac{i}{4}\hat{P}^+\left[b^* \frac{\partial}{\partial x}(b'^2) - \frac{\partial}{\partial x}(b^{*\prime}\frac{\partial}{\partial x}b^2)\right] \\ & -\frac{1}{2}\hat{P}^+\left[b\cdot\hat{k}(|b'|^2) - \frac{\partial}{\partial x}(b'\hat{k}(|b|^2))\right] \end{aligned} \tag{56}$$

Transformation from $b(x,t)$ to physical variables $\eta(x,t)$ and $\psi(x,t)$ can be recovered from canonical transformation. Here we write this transformation up to the second order:

$$\begin{aligned} & \eta(x) = \frac{1}{\sqrt{2}g^{\frac{1}{4}}}(\hat{k}^{\frac{1}{4}}b(x) + \hat{k}^{\frac{1}{4}}b(x)^*) + \frac{\hat{k}}{4\sqrt{g}}[\hat{k}^{\frac{1}{4}}b(x) - \hat{k}^{\frac{1}{4}}b^*(x)]^2, \psi(x) = \\ & -i\frac{g^{\frac{1}{4}}}{\sqrt{2}}(\hat{k}^{-\frac{1}{4}}b(x) - \hat{k}^{-\frac{1}{4}}b(x)^*) + \frac{i}{2}[\hat{k}^{\frac{1}{4}}b^*(x)\hat{k}^{\frac{3}{4}}b^*(x) - \hat{k}^{\frac{1}{4}}b(x)\hat{k}^{\frac{3}{4}}b(x)] \\ & +\frac{1}{2}\hat{H}[\hat{k}^{\frac{1}{4}}b(x)\hat{k}^{\frac{3}{4}}b^*(x) + \hat{k}^{\frac{1}{4}}b^*(x)\hat{k}^{\frac{3}{4}}b(x)]. \end{aligned}$$

Here $\hat{H}$ - is Hilbert transformation with eigenvalue $isign(k)$.

3.5 Modulational instability of wave train

We performed numerical simulation of the modulational instability of the homogeneous wavetrain in the framework of compact Eq.(56). Initial steepness of the wave train was equal to $\mu = 0.095$. This value was chosen for comparison with the earlier simulation in the framework of fully nonlinear

simulation [R82], [R83]. One can see in Fig.45 and Fig.46 that both waves coincide in details. Different time of their appearance is due to slightly different values of perturbations.

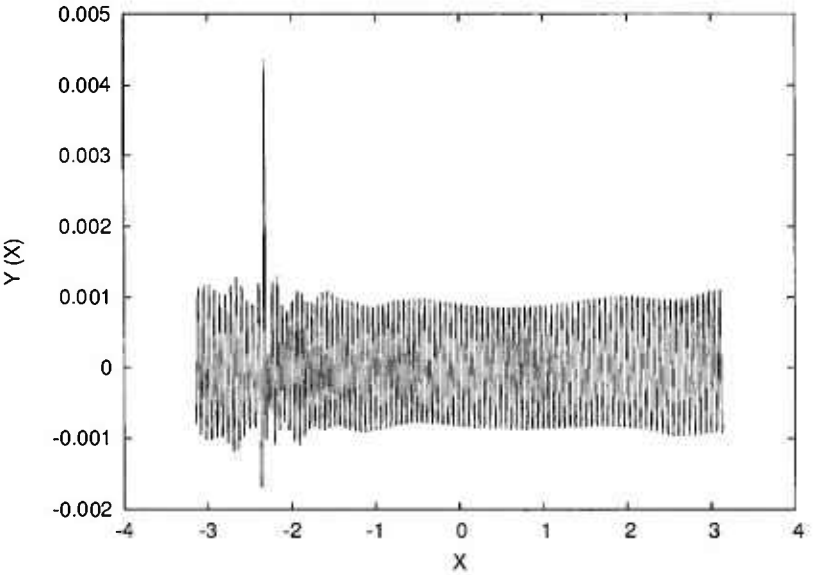

Fig.45 Freak-wave formation after t=802 (fully nonlinear equation)

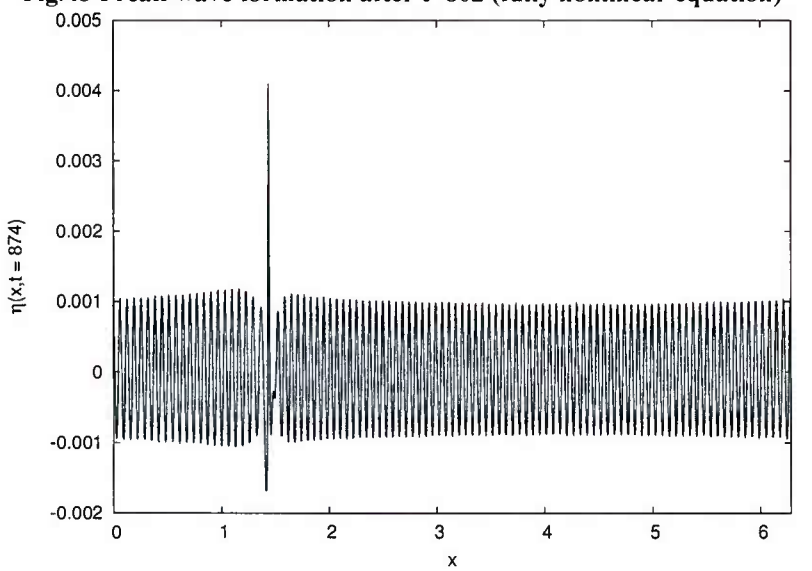

Fig.46 Freak-wave formation after t=874 (compact equation)

3.6 Breathers

We have also performed simulations of narrow breathers both in the framework of fully nonlinear conformal Eq.(55) and compact Eq.(56). Figs.47, 48 present pictures of the steepness of the surface of the fluid:

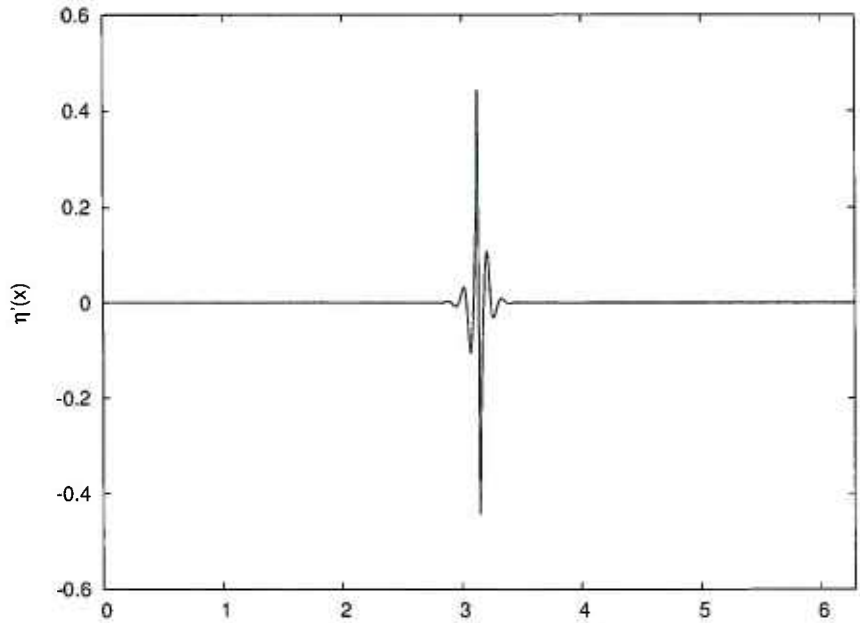

Fig.47 Steepness of the breather (compact equation).

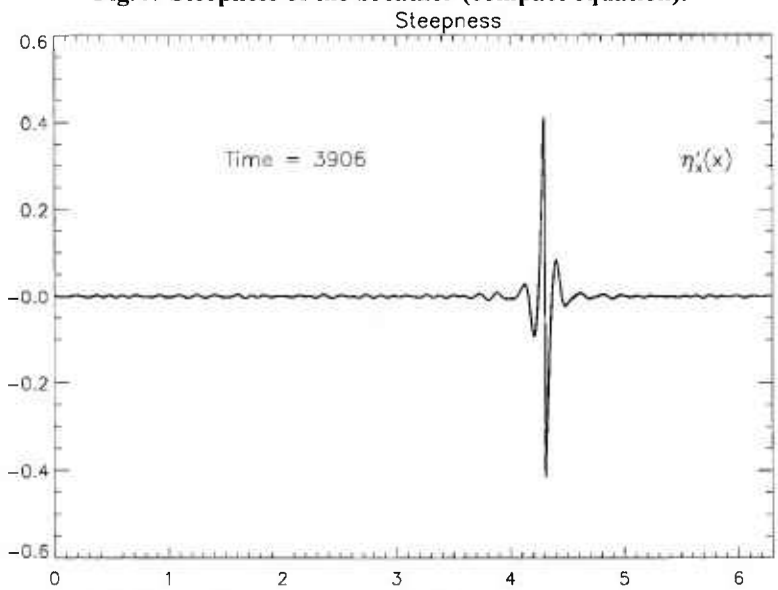

Fig.48 Profile of steepness (fully nonlinear equations).

We have demonstrated that compact equation, although approximate, quantitatively describes strongly nonlinear phenomena at the surface of potential fluid. We also have studied especially nonlinear stage of modulational instability up to the freak-wave formation and propagation of very steep breather.

3.7 Confirmed hypothesis of long-wave dissipation insignificance

Dissipation of water waves with JONSWAP initial spectral energy distribution was studied in the framework of compact Dyachenko-Zakharov equation

$$i\frac{\partial b}{\partial t} = \hat{\omega}_k b + \frac{i}{8}\left[b^* \frac{\partial}{\partial x}(b'^2) - \frac{\partial}{\partial x}(b^* \frac{\partial}{\partial x} b^2) \right] - \frac{1}{4}\left[b \cdot \hat{k}(|b'|^2) - \frac{\partial}{\partial x}(b'\hat{k}(|b|^2)) \right].$$

Different wind speeds from 9 to 20 m/sec were considered, with very long fetch of 157 km length. These experiments confirmed the hypothesis of long-wave dissipation insignificance due to wave-breaking **[P1,P2]**.

Typical behavior of energy density as a function of time is shown for wind speed 12 m/sec on Fig.49

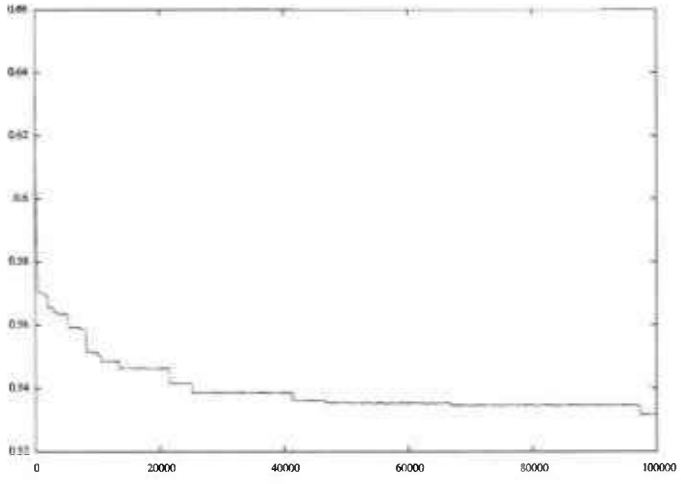

Fig.49 Energy (m^2) as a function of time (sec) for wind speed 12 m/sec .

One can see that dissipation takes place very rare and randomly. Drop of energy corresponds to wave breaking. This breaking leaves main core of energy spectrum unchanged. Average dissipation function is shown in Fig.50 for wind speed 12 m/sec. Also dissipation function used in *WAM3* and *WAM4* operational models is shown. Obviously, dissipation rate calculated in our experiments is much less than that of *WAM3* and *WAM4*:

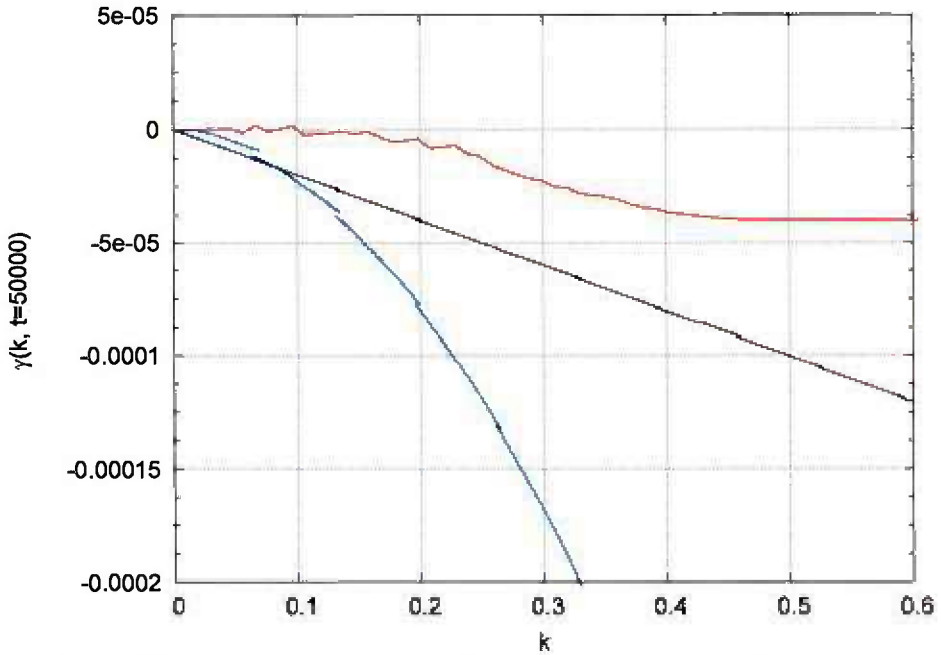

Fig.50 Dissipation of energy as a function of wavenumber *k* for dynamical model (blue line), *WAM3* model (red line) and *WAM4* model (black line)

3.8 Summary

The research results are published in [P13]-[P20].

4. Modulational instability and its implications for solitons, rogue waves and air-surface interactions

We studied the phenomenon of modulational instability. According to recent studies, the modulational instability seems to be a mechanism that is responsible for a number of phenomena that takes place in the ocean. In particular, experimental and numerical works have shown that the wave breaking mechanism and the formation of rogue waves may be caused by the modulational instability process.

In [P21] we have performed direct numerical simulation of the Navier-Stokes equations for simulating a two-phase flow (water and air) to study the dynamics of the modulational instability of free surface waves and its contribution to the interaction between the ocean and atmosphere.

If the steepness of the initial wave exceeds a threshold value, we observed wave-breaking events and the formation of large-scale dipole structures in the air. Because of the multiple steepening and breaking of the waves under unstable wave packets, a train of dipoles is released in the atmosphere; those dipoles propagate at a height comparable with the wavelength. The amount of energy dissipated by the breaker in water and air is considered, and contrary to expectations, we have observed that the

energy dissipation in air is greater than that in water. The possible implications for the wave modeling of aerosols and gases exchange between air and water are also discussed in the paper.

In [P22] the rogue wave solutions (rational multi-breathers) of the nonlinear Schrodinger equation (NLS) are tested in numerical simulations of weakly nonlinear and fully nonlinear hydrodynamic equations. A higher accuracy of wave propagation in space is reached using the modified NLS equation, i.e. Dysthe equation. This numerical modeling allowed us to directly compare simulations with recent results of laboratory measurements. In order to achieve even higher physical accuracy, we employed fully nonlinear simulations of potential Euler equations. These simulations provided us with basic characteristics of long time evolution of rational solutions of the NLS equation in the case of near-breaking conditions. The analytic NLS solutions are found to describe the actual wave dynamics of steep waves reasonably well.

In paper [P23] the problem of existence of stable nonlinear groups of gravity waves in deep water is considered by means of laboratory and numerical simulations with the focus on strongly nonlinear waves. Wave groups with steepness up to 0.30 are reproduced in laboratory experiments. We show that the groups remain stable and exhibit neither noticeable radiation nor structural transformation for more than 60 wavelengths or about 15-30 group lengths. These solitary wave patterns differ from the conventional envelope solitons, as only a few individual waves are contained in the group. Very good agreement is obtained between the laboratory results and numerical simulations of the potential Euler equations. The envelope soliton solution of the nonlinear Schrodinger equation is shown to be a reasonable first approximation for specifying the wave-maker driving signal. The short intense envelope solitons possess vertical asymmetry similar to regular Stokes waves with the same frequency and crest amplitude. Nonlinearity is found to have remarkably stronger effect on the speed of envelope solitons in comparison to the nonlinear correction to the Stokes wave velocity.

In paper [P24] we show experimentally that a stable wave propagating into a region characterized by an opposite current may become modulationally unstable. Experiments have been performed in two independent wave tank facilities; both of them are equipped with a wave-maker and a pump for generating a current propagating in the opposite direction with respect to the waves. The experimental results support a recent conjecture based on a current-modified nonlinear Schrodinger equation which establishes that rogue waves can be triggered by a non-homogeneous current characterized by a negative horizontal velocity gradient.

The paper [P25] is a review paper on rogue waves in different physical aspects ranging from

oceanography to nonlinear optics.

In the paper [P26] we present the first observation of dark solitons on the surface of water. It takes the form of an amp6itude drop of the carrier wave which does not change shape in propagation. The shape and width of the soliton depend on the water depth, carrier frequency, and the amplitude of the background wave. The experimental data taken in a water tank show an excellent agreement with the theory. These results may improve our understanding of the nonlinear dynamics of water waves at finite depths.

In paper [P27] we highlight an analogy between water waves and electromagnetic waves, i.e. the formation of a supercontinuum: starting from a very narrow band spectrum, after a few wave lengths, a very broad continuum spectrum (supercontinum) is observed with a consequent emission of solitons.

4. Acknowledgements

This research was supported by ONR grant N00014-10-1-0991. The authors gratefully acknowledge the support of this foundation.

References

[R1] V. E. Zakharov, D. Resio, A. Pushkarev, New wind input term consistent with experimental, theoretical and numerical considerations, arXiv:1212.1069 [physics.ao-ph], submitted for publication in JPO.

[R2] K. Hasselmann, On the non-linear energy transfer in a gravity-wave spectrum. Part I. General theory, Journal of Fluid Mechanics 12 (1962) 481 –500.

[R3] K. Hasselmann, On the non-linear energy transfer in a gravity wave spectrum Part 2. conservation theorems; wave-particle analogy; irrevesibility, Journal of Fluid Mechanics 15 (1963) 273 – 281.

[R4] I. R. Young, Wind Generated Ocean Waves, Elsevier, 1999.

[R5] G. J. Komen, L. Cavaleri, M. Donelan, K. Hasselmann, S. Hasselmann, P. A. E. Janssen, Dynamics and Modeling of Ocean Waves, Cambridge University Press, 1994.

[R6] P. Janssen, The Interaction of Ocean Waves and Wind, Cambridge monographs on mechanics and applied mathematics, Cambridge U.P., 2009.

[R7] V. E. Zakharov, Energy balances in a wind-driven sea, Physica Scripta, T142 (2010) 014052.

[R8] A. Pushkarev, D. Resio, V. Zakharov, Weak turbulent approach to the wind-generated gravity sea waves, Physica D 184 (2003) 29 – 63.

[R9] B. Tracy, D. Resio, Theory and calculation of the nonlinear energy transfer between sea waves in deep water, WIS report 11, U.S. Army Engineer Waterways Experiment Station, Vicksburg, MS, 1982.

[R10] D. J. Webb, Non-linear transfers between sea waves, Deep-Sea Res., 25 (1978) 279 – 298.

[R11] I. V. Lavrenov, Wind-waves in oceans: dynamics and numerical simulations, Springer, 2010.

[R12] K. Komatsu, A. Masuda, A new scheme of nonlinear energy transfer among wind waves: RIAM method. algorithm and performance, Journal of Oceanography 52 (1996) 509 – 537.

[R13] H. U. Sverdrup, W. H. Munk, Wind, sea and swell: theory of relations for forecasting, Vol. H.O. Pub. No. 601, US HYDROGRAPHIC OFFICE, 1947.

[R14] V. E. Zakharov, V. S. L'vov, G. Falkovich, Kolmogorov Spectra of Turbulence I: Wave Turbulence, Springer-Verlag, 1992.

[R15] V. E. Zakharov, Theoretical interpretation of fetch-limited wind-driven sea observations, NPG 13 (2005) 1 – 16.

[R16] S.I. Badulin, A.N. Pushkarev, D.Resio, V.E. Zakharov, Self-similarity of wind-driven sea, Nonlinear Proc. in Geophysics 12 (2005) 891 – 945.

[R17] S. I. Badulin, A. Babanin, D. Resio, V. E. Zakharov, Weakly turbulent laws of wind-wave growth, JFM 591 (2007) 339 – 378.

[R18] E. Gagnaire-Reno, M. Benoit, S. Badulin, On weakly turbulent scaling of wind sea in simulation of fetch-limited growth, JFM 669 (2011) 178 – 213.

[R19] V. E. Zakharov, S. I. Badulin, P. A. Hwang, G. Caulliez, Universality of sea wave growth and its physical roots, arXiv:1411.7235 [physics.ao-ph] (2014), submitted в Journal of Fluid Mechanics 09.24.2014

[R20] V. Zakharov, S.I.Badulin, On energy balance in wind-driven sea, Doklady Akademii Nauk 440 (2011) 691 – 695.

[R21] G. J. Komen, S. Hasselmann, K. Hasselmann, On the existence of a fully developed wind-sea spectrum, J. Phys. Oceanogr. 14 (1984) 1271 – 1285.

[R22] S. E. Belcher, J. C. R. Hunt, Turbulent flow over hills and waves, Annual Review of Fluid Mechanics 30 (1998) 507 – 538.

[R23] D. V. Chalikov, V. K. Makin, Models of the wave boundary layer, Boundary-Layer Meteorology 56 (1991) 83 – 99.

[R24] V. N. Kudryavtsev, V. K. Makin, J. F. Meirink, Simplified model of the air flow above the waves, Boundary-Layer Meteorology 98 (2001) 155 – 171.

[R25] H. L. Tolman, D. Chalikov, Source terms in a third-generation wind-wave model, JPO 26 (1996) 2497 – 2518.

[R26] J. Miles, On the generation of surface waves by shear flows, JFM 3 (1957) 185 – 204.

[R27] H. Jeffreys, On the formation of water waves by wind, Proc. Roy. Soc. 107A (1924) 189 – 206.

[R28] H. Jeffreys, On the formation of water waves by wind ii, Proc. Roy. Soc. 107A (1925) 341 – 347.

[R29] Y. Troitskaya, D. Sergeev, O. Ermakova, G. Balandina, Statistical parameters of the air boundary layer over steep water waves measured by pivtechnique, JPO 41 (2011) 1421 – 1454.

[R30] A. Fabricant, Quasilinear theory of wind-waves generation, Izv. Atmos. Ocean. Phys. 12 (1976) 858 – 862.

[R31] Y. L. Nikolaeva, L. S. Zymring, Kinetic model of sea wind waves generation by turbulent wind, Izv. Atmos. Ocean. Phys. 22 (1986) 135 – 142.

[R32] P. A. E. M. Janssen, Quasilinear approximation for the spectrum of wind-generated water waves, JFM 117 (1982) 493 – 506.

[R33] T. S. Hristov, S. D. Miller, C. A. Friehe, Dynamical coupling of wind and ocean waves through wave-induced air flow, Nature 422 (2003) 55 – 58.

[R34] M. Donelan, A. V. Babanin, I. R. Young, M. Banner, Waves-follower field measurements of the wind-input spectral function. Part II: Parameterization of the wind input, JPO 36 (2006) 1672 – 1689.

[R35] D. Chalikov, The parameterization of the wave boundary layer, JPO 25 (1995) 1333 – 1349.

[R36] W. J. Plant, A relationship between wind stress and wave slope, JGR 87 (1982) 1961 – 1967.

[R37] C. Mastenbroek, V. K. Makin, M. H. Garat, J. P. Giovanangeli, Experimental evidence of the rapid distortion of turbulence in the air flow over water waves, JFM 318 (1996) 273 – 302.

[R38] M. Donelan, A. V. Babanin, I. R. Young, M. L. Banner, C. McCormick, Wave-follower field measurements of the wind-input spectral function. Part I: Measurements and calibrations, J. Atmos. Oceanic Technol. 22 (2005) 799–813.

[R39] I. R. Young, A. V. Babanin, Spectral distribution of energy dissipation due to dominant wave breaking, JPO 36 (2006) 376 – 394.

[R40] R. L. Snyder, F. W. Dobson, J. A. Elliott, R. B. Long, Array measurements of atmospheric pressure fluctuations above surface gravity waves, JFM 102 (1981) 1 – 59.

[R41] S. V. Hsiao, O. H. Shemdin, Measurements of wind velocity and pressure with a wave follower during MARSEN, JGR 88 (1983) 9841 – 9849.

[R42] D. Hasselmann, J. Bosenberg, Field measurements of wave-induced pressure over wind-sea and swell, JFM 230 (1991) 391 – 428.

[43] WAMDI-Group, The WAM model - a third generation ocean wave prediction model, J. Phys. Oceanogr. 18 (1988) 1776 – 1810.

[R44] A. Pushkarev, V. Zakharov, Quasibreathers in the MMT model, Physica D 248 (2013) 55 – 61.

[R45] K. Tsagareli, A. Babanin, D. Walker, I. Young, Numerical investigation of spectral evolution of wind waves, JPO 40 (2009) 656 – 666.

[R46] P. A. Hwang, Spectral signature of wave breaking in surface wave components of intermediate-length scale, Journal of Marine Systems 66 (2007) 28–37.

[R47] P. A. Hwang, D. W. Wang, An empirical investigation of source term balance of small scale surface waves, Geophys. Res. Lett. 31 (2004) L15301.

[R48] P. Hwang, Y. Toporkov, M. Sitten, S. Menk, Measuring wave breaking by radar, WISE meeting, College Park, MD, USA, 2013.

[R49] P. Huang, Y. Toporkov, M. Sitten, S. Menk, Mapping surface currents and waves with interoferomic synthetic aperture radar in coastal waters: observation of wave breaking in swell–dominant conditions, JPO (2013) 563–581.

[R50] H. L. Tolman, User manual and system documentation of WAVEWATCH III, Environmental Modeling Center, Marine Modeling and Analysis Branch.

[R51] V. E. Zakharov, A. O. Korotkevich, A. O. Prokofiev, On Dissipation Function of Ocean Waves due to Whitecapping, in: T. E. Simos, G. Psihoyios, C. Tsitouras (Eds.), American Institute of Physics Conference Series, Vol.1168 of American Institute of Physics Conference Series, 2009, pp. 1229–1231. doi:10.1063/1.3241292.

[R52] V. E. Zakharov, D. I. Kachulin, A. I. Dyachenko, On dissipation of ocean spectra due to wave-breaking, accepted fo publication in Doklady of RAS 102

[R53] O.M. Phillips, The dynamics of the upper ocean (1966).

[R54] O. M. Phillips, Spectral and statistical properties of the equilibrium range in wind-generated gravity waves, JFM 156 (1985) 505 – 531.

[R55] A. C. Newell, V. E. Zakharov, The role of the generalized phillips' spectrum in wave turbulence, Physics Letters A 372 (2008) 4230 – 4233.

[R56] S. I. Badulin, V. E. Zakharov, The generalized Phillips' spectra and new dissipation function for wind-driven seas, arXiv:1212.0963 [physics.ao-ph] (2012) 1 – 16, , Ocean Modelling, submitted 02.18.2015.

[R57] D. Resio, C. Long, Equilibrium-range constant in wind-generated spectra, JGR 109 (2004) CO1018.

[R58] C. Long, D. Resio, Wind wave spectral observations in Currituck Sound, North Carolina, JGR 112 (2007) C05001.

[R59] W. Perrie, V. Zakharov, The equilibrium range cascades of wind-generated waves, Eur. J. Mech. B/Fluids 18 (1999) 365 – 371.

[R60] D. Resio, W. Perrie, Implications of an f4 equilibrium range for windgenerated waves, JPO 19 (1989) 193 – 204.

[R61] D. T. Resio, C. E. Long, C. L. Vincent, Equilibrium-range constant in wind-generated wave spectra, JGR 109 (2004) CO1018.

[R62] D. Resio, C. Long, Equilibrium-range constant in wind-generated spectra, JGR 109 (2004) CO1018.

[R63] C. Long, D. Resio, Wind wave spectral observations in Currituck Sound, North Carolina, JGR 112 (2007) C05001.

[R64] A. O. Korotkevich, A. N. Pushkarev, D. Resio, V. E. Zakharov, Numerical verification of the weak turbulent model for swell evolution, Eur. J. Mech. B - Fluids 27 (2008) 361 – 387.

[65] V. Zakharov, N. N. Filonenko, The energy spectrum for stochastic oscillations of a fluid surface, Sov. Phys. Docl. 11 (1967) 881 – 884.

[R66] M. M. Zaslavski, V. E. Zakharov, The kinetic equation and Kolmogorov spectra in the weak turbulence theory of wind generated waves, Proc. Acad. Scien. USSR 18 (1982) 970 – 980.

[R67] V. E. Zakharov, Direct and inverse cascade in wind – driven sea and wavebreaking, in: M. L. Banner, R. H. Y. Grimshaw (Eds.), Proceedings of IUTM Meeting on Wave Breaking, Sydney, 1991, Springer-Verlag, 1992, pp. 69 – 91.

[R68] V. E. Zakharov, Statistical theory of surface waves on fluid of finite depth, Eur. J. Mech. B/Fluids 18 (1999) 327 – 344.

[R69] Y. Toba, Local balance in the air-sea boundary processes, Journal of the Oceanographical Society of Japan 29 (1973) 209 – 220.

[R70] S. I. Badulin and V. G. Grigorieva, On discriminating swell and wind-driven seas in Voluntary Observing Ship data. Journal of Geophysical Research, Vol. 117, C00J29, doi:10.1029/2012JC007937, 2012

[R71] Badulin, S. I. (2014), A physical model of sea wave period from altimeter data, J. Geophys. Res. Oceans, 119, doi:10.1002/2013JC009336. - IF - 3.44

[R72] Donelan,M. A. and Pierson-jr.,W. J.: Radar scattering and equilibrium ranges in wind-generated waves with application to spectrometry, J. Geoph. Res., 92, 49715029, 1987.

[R73] Gulev, S. K., V. Grigorieva, A. Sterl, and D. Woolf, Last century changes in ocean wind wave height from global visual wave data, Geophys. Res. Lett., 31, L24302, 2004, doi:10.1029/2004GL021040

[R74] Gulev, S.K. and V. Grigorieva Last century changes in ocean wind wave height from global visual wave data. Geophys. Res. Lett , 2004

[R75] Hasselmann, K., Ross, D. B., Muller, P. & Sell, W. 1976 A parametric wave prediction model. *J. Phys. Oceanogr.* **6**, 200–228.

[R76] Zakharov, V. E. & Zaslavsky, M. M. 1983*b* Dependence of wave parameters on the wind velocity, duration of its action and fetch in the weak-turbulence theory of water waves. *Izv.Atmos. Ocean. Phys.* **19** (4), 300–306.

[R77] Laugel, A., M. Benoit, and G. Mattarolo, ANEMOC-2: Construction of a 31-year hindcast sea-state database over the Atlantic Ocean, calibration based on altimeter observations from 2000 to 2009, paper presented at 19th International Conference Waves In Shallow Environments, Politech. Univ. of Catalonia, Barcelona, Spain, 16–20 Apr., 2012

[R78] Gommenginger, C. P., M. A. Srokosz, P. G. Challenor, and P. D. Cotton, Measuring ocean wave period with satellite altimeters: A simple empirical model, *Geophys. Res.Lett.*, *30* (22), 2150, doi:10.1029/ 2003GL017743, 2003.

[R79] Quilfen, Y., B. Chapron, and M. Serre, Calibration/validation of an altimeter wave period model and application to TOPEX/Poseidon and Jason-1 altimeters, *Marine Geodesy*, *27*, 535–549, 2004.

[R80] Badulin, S. I., Babanin, A. V., Resio, D., Zakharov V., Numerical verification of weakly turbulent law of wind wave growth. In *IUTAM Symposium on Hamiltonian Dynamics, Vortex Structures, Turbulence. Proceedings of the IUTAM Symposium held in Moscow, 25-30 August, 2006* (ed. A. V. Borisov, V. V. Kozlov, I. S. Mamaev & M. A. Sokolovskiy), *IUTAM Bookseries*, vol. 6, pp. 175–190. Springer, ISBN: 978-1-4020-6743-3, 2008

[R81] Dyachenko, A.I.: On the dynamics of an ideal fluid with a free surface. Doklady Mathematics, 63(1), 115—118, 2001

[R82] Dyachenko, A.I. and Zakharov, V.E.: Modulation Instability of Stokes Wave → Freak Wave, JETP Letters, 81(6), 255—259, 2005

[R83] Zakharov, V.E., Dyachenko, A.I. and Prokofiev, A.O.: Freak waves as nonlinear stage of Stokes wave modulation instability, European Journal of Mechanics B/Fluids, v. 120(5), 677 – 692, 2006

Publications

[P1] V. E. Zakharov, D. Resio, A. Pushkarev, New wind input term consistent with experimental, theoretical and numerical considerations, arXiv:1212.1069 [physics.ao-ph], (2013), submitted to JPO

[P2] A.N. Pushkarev, V.E. Zakharov, On nonlinearity implications and wind forcing in Hasselmann equation, arXiv:1503.07091 [physics.ao-ph], (2015)

[P3] A.N. Pushkarev, V.E. Zakharov, Comparison of wind input terms in Hasselmann equation, submitted to Ocean Modeling

[P4] A.N. Pushkarev, V.E. Zakharov, Quasibreathers in the MMT model, Physica D 248 (2013) 55 – 61

[P5] E. Gagnaire-Reno, M. Benoit, S. Badulin, On weakly turbulent scaling of wind sea in simulation of fetch-limited growth, JFM 669 (2011) 178 – 213.

[P6] V. E. Zakharov, S. I. Badulin, P. A. Hwang, G. Caulliez, Universality of sea wave growth and its physical roots, arXiv:1411.7235 [physics.ao-ph] (2014), submitted to Journal of Fluid Mechanics

[P7] V. Zakharov, S.I.Badulin, On energy balance in wind-driven sea, Doklady Akademii Nauk 440 (2011) 691 – 695.

[P8] V. E. Zakharov, S. I. Badulin, P. A. Hwang, G. Caulliez, Universality of sea wave growth and its physical roots, arXiv:1411.7235 [physics.ao-ph] (2014), submitted в Journal of Fluid Mechanics

[P9] V. Zakharov, S.I.Badulin, On energy balance in wind-driven sea, Doklady Akademii Nauk 440 (2011) 691 – 695.

[P10] S. I. Badulin, V. E. Zakharov, The generalized Phillips' spectra and new dissipation function for wind-driven seas, arXiv:1212.0963 [physics.ao-ph] (2012), 1 – 16, submitted to Ocean Modelling.

[P11] S. I. Badulin and V. G. Grigorieva, On discriminating swell and wind-driven seas in Voluntary Observing Ship data. Journal of Geophysical Research, Vol. 117, (2012), C00J29, doi:10.1029/2012JC007937,

[P12] Badulin, S. I. A physical model of sea wave period from altimeter data, J. Geophys. Res. Oceans, 119, (2014)

[P13] Dyachenko, A.I. and Zakharov, V.E.: Compact equation for gravity waves on deep water, JETP Letters, 93(12), 701—705, 2011

[P14] Dyachenko, A.I., Zakharov, V.E.: A dynamic equation for water waves in one horizontal dimension. Europ. J. Mech. B 32, 17—21, 2012

[P15] A.I. Dyachenko, D.I. Kachulin, V.E. Zakharov "On dissipation of the gravity waves due to wave-breaking", accepted for publication in JETP Letters

[P16] D.I Kachulin, V.E Zakharov, A.I Dyachenko, Dissipation of water waves and breakers. International conference Landau days 2015, Chernogolovka, Russia, June 22-25, 2015

[P17] A.I. Dyachenko, D.I. Kachulin, V.E. Zakharov, On dissipation of the gravity waves due to wave-breaking, accepted for publication in JETP Letters

[P18] V. E. Zakharov, A. V. Odesskii, M. Cisternino, and M. Onorato, Five-wave classical scattering matrix and integrable equations, Theoretical and Mathematical Physics, 180(1): 759–764 (2014)

[P19] A.I. Dyachenko, D.I. Kachulin, and V.E. Zakharov, On the non-integrability of the free surface hydrodynamics, JETP Lett., 98(1), 43-47, (2013).

[P20] A.I. Dyachenko and V.E. Zakharov, A dynamic equation for water waves in one horizontal dimension, Eur. J. Mech. B/Fluids, 32, 17-21, (2012).

[P21] A. Iafrati, A. Babanin, and M. Onorato, Modulational Instability, Wave Breaking, and Formation of Large-Scale Dipoles in the Atmosphere, Phys. Rev. Lett. 110, 184504, 2013

[P22] A. Slunyaev, E. Pelinovsky, A. Sergeeva, A. Chabchoub, N. Hoffmann, M. Onorato, and N. Akhmediev, Super-rogue waves in simulations based on weakly nonlinear and fully nonlinear hydrodynamic equations, Phys. Rev. E 88, 012909, 2013

[P23] Slunyaev, A.; Clauss, G. F.; Klein, M.; Onorato, M., Simulations and experiments of short intense envelope solitons of surface water waves, Physics of Fluids, Volume 25, Issue 6, pp. 067105-067105-16 (2013)

[P24] A. Toffoli, T. Waseda, H. Houtani, T. Kinoshita, K. Collins, D. Proment, and M. Onorato, Excitation of rogue waves in a variable medium: An experimental study on the interaction of water waves and currents, Phys. Rev. E 87, 051201(R), 2013

[P25] M. Onorato, S. Residoric, U. Bortolozzo, A. Montina, F.T. Arecchi, Rogue waves and their generating mechanisms in different physical contexts, Volume 528, Issue 2, 47–89, 2013

[P26] A. Chabchoub, O. Kimmoun, H. Branger, N. Hoffmann, D. Proment, M. Onorato, and N. Akhmediev, Experimental Observation of Dark Solitons on the Surface of Water, Phys. Rev. Lett. 110, 124101, 2013

[P27] A. Chabchoub, O. Kimmoun, H. Branger, C. Harif, N. Hoffmann, M. Onorato and N. Akhmediev, Gray solitons on the surface of water, Physical Review E-Statistical, Nonlinear and Soft Matter Physics, vol. 89, no. 1, pp. 011002(R), (2014).